Christie, D.M., Pedersen, R.B., Miller, D.J., et al., 2001
Proceedings of the Ocean Drilling Program, Initial Reports Volume 187

8. Site 1157[1]

Shipboard Scientific Party[2]

PRINCIPAL RESULTS

Site 1157 is located in Zone A, ~55 km east of the ~127°E fracture zone that bounds the eastern Australian Antarctic Discordance (AAD) and 230 km south of Site 1153, which is on approximately the same flow line. It is ~100 km southeast of Site 1156, on seafloor of the same age (~22 Ma). The purpose of drilling at this site, together with Site 1158, and the other western Zone A sites was to test for occurrences of Indian-type mantle beneath Zone A.

Hole 1157A was spudded in ~5069 m water depth and was washed through ~200 m of dark to medium brown siliceous clay. Rotary drilling continued 16.4 m into basement, recovering 2.9 m (~17.8%) of rubble made up of basalt and basalt-carbonate breccia. Both aphyric and moderately plagioclase-olivine phyric basalts are present. The breccia is composed of angular fragments of basalt (3 to >8 cm), basaltic glass, and palagonite in a carbonate matrix. Low-temperature alteration halos rim many clasts, and some terminate at broken clast surfaces, indicating that alteration of these clasts preceded the final brecciation.

After Hole 1157A was abandoned because of drilling problems, Hole 1157B was spudded 200 m to the west and was washed through 130.6 m of sediments with no recovery. The hole continued 40.4 m into basement, recovering 11.7 m (29%) of sparsely to moderately plagioclase-olivine phyric pillow basalt with a moderate degree of low-temperature alteration.

Six glass and whole-rock samples range in MgO content from 8.4 to 6.6 wt%. As in all previous sites, the whole rocks have lower MgO contents than the glasses. At Site 1157, Fe_2O_3, TiO_2, Zr, and Y contents are low relative to the near-axis dredge samples from Zone A, whereas at Site 1153, which is 5 m.y. older, these elements are high. These temporal fluctuations indicate a complex spectrum of accretionary processes near the eastern margin of the depth anomaly and the isotopic bound-

[1]Examples of how to reference the whole or part of this volume.
[2]Shipboard Scientific Party addresses.

Ms 187IR-108

ary. Ba and Zr contents suggest an Indian-type mantle source for lavas at Site 1157. This was the first Indian trace element signature that we observed in Zone A.

OPERATIONS

Transit to Site 1157

The sixth site of Leg 187 is 50 nmi southwest of Site 1156. Our transit took 4.3 hr at an average speed of 11.6 kt. At 1315 hr on 12 December, we slowed to 5 kt to conduct a single-channel seismic (SCS) survey.

Hole 1157A

We deployed a positioning beacon about 1.6 km east of the prospectus Global Positioning System (GPS) coordinates where our survey indicated a 200-m sediment thickness. Water depth at this site is 5080.4 m below the rig floor, determined by the precision depth recorder (PDR). A new C-7 four-cone rotary bit was installed on the same nine-collar bottom-hole assembly used at our previous sites. We started washing through the sediment column at Hole 1157A at 2300 hr on 12 December and continued to 200.0 meters below seafloor (mbsf), where drilling conditions indicated we had reached basement. A single wash barrel was recovered, and we cored from 200.0 to 216.4 mbsf before we decided, based on poor drilling conditions and recovery (Table T1), to abandon the hole. We deployed fluorescent microspheres as a tracer for microbiological infiltration analysis on Core 1157A-2R. The drill string cleared the seafloor at 1300 hr on 13 December; we offset 200 m west to drill Hole 1157B.

T1. Coring summary, Site 1157, p. 54.

Hole 1157B

We initiated Hole 1157B by washing down to 130.6 mbsf before hitting basement. Coring continued from 130.6 to 171.0 mbsf with an average recovery of 29%. Microbiological tracers were deployed on Cores 1157B-2R and 9R. After ~34 m of penetration and 10 m of recovered basalt, we concluded operations at this site. The bit cleared the seafloor at 0225 hr and the rotary table at 1045 hr on 15 December.

IGNEOUS PETROLOGY

Introduction

Holes 1157A and 1157B were cored into igneous basement from 200.0 to 216.4 and 130.6 to 171.0 mbsf, respectively. Hole 1157A (Sections 187-1157A-2R-1 through 4R-1) was drilled 16.40 m into basement, resulting in 2.92 m (17.8%) recovery. All recovered material from this hole has been assigned to one lithologic unit: basaltic rubble with intervals of basalt-carbonate breccia. The unit is composed of poorly sorted lithic clasts, derived from aphyric basalt and moderately plagioclase-olivine phyric basalt. The material is interpreted as a talus pile; no primary magmatic stratigraphic significance can be associated with the position of individual pieces in the hole.

Hole 1157B (Sections 187-1157B-2R-1 through 9R-1) was drilled 40.4 m into basement, resulting in 11.70 m (28.96%) recovery. Lavas from

this hole were assigned to a single lithologic unit of moderately plagioclase-olivine phyric basalt. The unit is interpreted as basalt pillow lava, based on the abundance of glassy chilled margins recovered (i.e., 22% of all pieces), the presence of V-shaped pieces, and pieces with curved glassy rinds.

Hole 1157A

Unit 1

Unit 1 of Hole 1157A consists of basaltic rubble with two intervals of basalt-carbonate breccia (Section 187-1157A-2R-1 [Pieces 3–7] and Section 3R-1 [Pieces 12–19]). There are two different igneous lithologies among the rubble and breccia clasts: a dark gray aphyric basalt and a medium gray plagioclase-olivine phyric basalt. The two lithologies are present throughout the hole in roughly equal proportions. There is no apparent variation in relative proportions with depth in the hole, and both lithologies can be observed in the same piece of breccia in Section 187-1157A-3R-1 (Piece 6) (Fig. F1). Both basalt types are characterized by weathered outer surfaces and are slightly to moderately altered throughout the unit. Alteration is concentrated in halos that have formed adjacent to veins, fractures, and outer weathered surfaces and consists predominantly of replacement of olivine and groundmass by a mixture of Fe oxyhydroxides and clay (see "Alteration," p. 7). Although the alteration halos for most breccia clasts lie adjacent to the carbonate sediment matrix, not all clasts have alteration halos, indicating that the weathering and/or alteration responsible for the halos occurred before formation of the lithified rubble deposit.

F1. Basalt breccia containing clasts of aphyric and plagioclase-olivine phyric basalt, p. 14.

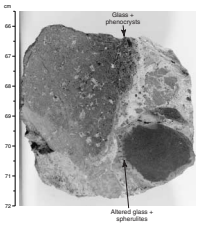

Petrography of Basaltic Rubble Clasts

Moderately Plagioclase-Olivine Phyric Basalt. The moderately plagioclase-olivine phyric basalt contains 1%–2% equant to skeletal olivine and 1%–6% tabular to prismatic plagioclase phenocrysts. Plagioclase is typically seriate and, although crystals range in size to 5 mm, most are <1–2 mm long. Larger crystals tend to have equant (subhedral) or rounded (anhedral) shapes. Sieve-textured plagioclase is common, although variable in character, ranging from crystals with only embayed cores to crystals with only embayed rims. Zoning is commonly discontinuous in sieve-textured plagioclase, but most crystals are unzoned. All plagioclase phenocrysts are twinned. In more altered areas, plagioclase crystals are stained along microcracks by Fe oxyhydroxides (see "Hole 1157A," p. 7, in "Alteration"); elsewhere plagioclase is unaltered. Olivine phenocrysts (0.5–3 mm) are present throughout and range from equant (subhedral to euhedral) to skeletal; they are present both in glomerocrysts in association with plagioclase and as discrete crystals. In alteration halos, olivine phenocrysts are partially to totally replaced by Fe oxyhydroxides and clay; elsewhere, they are usually unaltered (see "Hole 1157A," p. 7, in "Alteration").

Groundmass textures are microcrystalline and range from intersertal to immature sheaf quench morphologies. Acicular plagioclase (aspect ratios up to 40:1) forms as much as 30% of the groundmass; small (<100 µm) equant olivines form ~2% of the groundmass. In most cases, clinopyroxene is restricted to quench crystal morphologies intergrown with plagioclase sheafs. However, in some areas the crystallization of clinopyroxene is unusually enhanced, leading to formation of granular, anhedral clinopyroxene as large as 20 µm. In Sample 187-1157B-3R-1,

97–101 cm, small crystals of clinopyroxene have euhedral terminations on one end, indicating growth into a miarolitic cavity (Fig. F2) that is now filled with secondary calcite (see "Hole 1157A," p. 7, in "Alteration"). These cavities represent areas of volatile concentration during the final stage of crystallization, which would have facilitated the growth of clinopyroxene. Minute (<2 µm) equant opaque minerals make up ~1%–2% of the groundmass. Dark brown mesostasis—which here includes glass plus quench crystals of plagioclase, clinopyroxene, and olivine that are not readily distinguishable—constitutes >50% of the rock. Spherical vesicles are present in abundances of <1% and are typically very small (<50–100 µm in diameter); they are usually unfilled; but, in some altered areas, they are filled with calcite (see "Hole 1157A," p. 7, in "Alteration").

Aphyric Basalt. The aphyric basalt consists of <1% olivine microphenocrysts (0.3–0.8 mm) in a microcrystalline groundmass dominated by sheaf quench textures (Fig. F3). The olivine microphenocrysts are equant, and most are skeletal (Fig. F3). The groundmass consists of ~35% acicular plagioclase (aspect ratio up to 50:1), 1%–2% small (<100 µm) equant olivine (Fig. F3), and 1%–2% small (<20 µm) equant opaque minerals. Similar to the moderately plagioclase-olivine phyric basalts described above, the groundmass contains some areas in which clinopyroxene is present as larger, granular crystals rather than the more typical quench plumose morphologies. Although miarolitic cavities are not observed, the local enhancement of crystal growth suggests similar conditions for the evolution and liberation of volatiles during crystallization. As with the phyric basalts, these crystal clots are associated with secondary calcite. Dark brown, quench-textured mesostasis makes up >50% of the rock. Vesicles are usually small (<0.5 mm), uniformly distributed, and make up <1% of the rock; some are filled with calcite, but most are unfilled.

Chilled Margins. Chilled margins were recovered on nine of the rubble clasts (i.e., 18% of the pieces). Six of these are aphyric and three are phyric basalts. Few of the pieces retain a significant thickness of clear glass, and most consist of glass + spherulitic quench crystals. The zone of coalesced spherulites is typically thin (3–4 mm), and the spherulites are relatively small (~100 µm diameter). One exception is interval 187-1157A-3R-1, 124–132 cm, which is notable for its coarser spherulitic texture (individual spherulites as large as 2 mm) and wider chilled margin (>2.5 cm) (Fig. F4).

Petrography of the Breccia

There are two breccia intervals in Unit 1 of Hole 1157A (Section 187-1157A-2R-1 [Pieces 3–7] and Section 3R-1 [Pieces 12–19]). The breccias are poorly sorted and are cemented by a range of carbonate, carbonate + clay, and clay sediments and/or cements. The clasts are angular and range from sand-sized particles of palagonite and altered olivine to pieces of aphyric and moderately plagioclase-olivine phyric basalt that are larger than the diameter of the core (>8 cm). The petrography of the basalts is identical to the aphyric and phyric basalts described in detail above.

The matrix varies from a lithic-poor calcarenite (e.g., Section 187-1157A-2R-1; Fig. F5) to a lithic-rich (~80% lithic fragments) calcareous sediment (e.g., Section 187-1157A-3R-1; Fig. F6). In most places, the calcarenite is a mottled, pinkish gray. In thin section, it is seen to consist of >95% round to oval grains, each of which is a single calcite crystal (0.1–0.3 mm). The crystals are poorly cemented by interstitial clay (Fig.

F2. Euhedral clinopyroxene growth into a miarolitic cavity, now filled with calcite, p. 15.

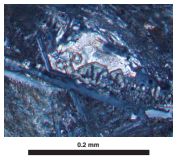

F3. Skeletal olivine microphenocrysts and plagioclase sheaf quench texture in aphyric basalt, p. 16.

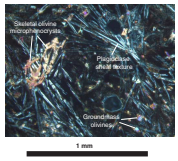

F4. Wide spherulitic chilled margin (between 124 and 128 cm), p. 17.

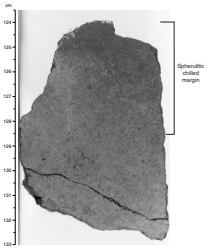

F5. Calcarenite sediment partially enclosing a plagioclase-olivine phyric basalt clast, p. 18.

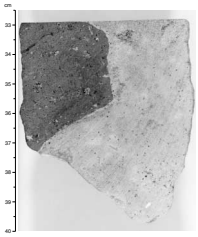

F6. Basalt breccia with lithic-rich calcareous sediment matrix, p. 19.

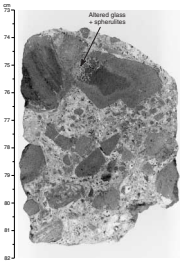

F7). The proportion of clay increases locally, and small (<2 mm) lithic fragments are concentrated in these clay-rich areas. Included among the lithic fragments are glass shards (unaltered and retaining quench crystals; Fig. F8) and palagonite. The latter varies in appearance from laminated (Fig. F9) to vermiform (Fig. F10). Also present are angular fragments of unaltered feldspar (<0.3 mm maximum dimension), but these constitute <1% of the lithic clasts. Mn oxide concretions as large as 0.3 mm are common throughout, but most are <<0.1 mm (Fig. F7A).

The lithic-rich calcareous sediment in Section 187-1157A-3R-1 (Fig. F6) is similar in appearance to the lithic-rich areas of the calcarenite described above but includes larger (e.g., 0.5–3 cm) clasts of slightly to moderately altered basalt (Fig. F6), as well as smaller fragments of palagonite and glass. Material associated with basaltic chilled margins (e.g., palagonite and altered spherulitic basalt) predominates. The fine-grained matrix consists of a mixture of pale pink to buff clay and micritic calcite crosscut by an anastomosing network of sparry calcite that encircles clasts, forms thin veins, and replaces both matrix and clasts.

Sediment was not recovered in significant volumes in Sections 187-1157A-3R-2 through 4R-1, but small remnant patches (a few millimeters to several centimeters across and <1 mm thick) of micritic calcite and/or clay are observed adhering to the outer surfaces of individual pieces. These patches and the ease with which the sediment matrix parts from the larger basaltic clasts suggest that the breccia sensu stricto may be underrepresented in the material recovered.

Hole 1157B

Unit 1

Petrography of Basalts

Unit 1 of Hole 1157B is a moderately plagioclase-olivine phyric basalt (Fig. F11), the petrography of which is very similar to the phyric basalts recovered in Hole 1157A. It consists of 1%–2% equant to skeletal olivine and 1%–6% tabular to prismatic plagioclase phenocrysts. The plagioclase phenocryst content varies unsystematically throughout the unit, with some pieces appearing nearly aphyric. Large plagioclase phenocrysts (up to 7 mm) are present, but most (>90%) average 2–3 mm in length. The larger crystals tend to have blocky (subhedral) to rounded (anhedral) shapes and are more likely to display discontinuous zoning as well as sieve textures (both embayed cores and embayed rims were observed). Smaller plagioclase phenocrysts are typically prismatic and unzoned, although there are sieve textures in these crystals as well. Many plagioclase phenocrysts are crosscut by microcracks that are stained with Fe oxyhydroxides (see "Hole 1157B," p. 8, in "Alteration"), but otherwise plagioclase is unaltered. Olivine phenocrysts are present throughout as equant (subhedral) to skeletal crystals, most of which are <2 mm in size, although crystals as large as 5 mm are observed. Outside of alteration halos, they are usually unaltered. Cr spinel is present in trace amounts, both as small (<50 µm) anhedral to subhedral inclusions in olivine and plagioclase and as larger (0.6 mm) euhedral microphenocrysts.

Between 10% and 30% of the phenocrysts are included in glomerocrysts of plagioclase, olivine, and plagioclase + olivine (± clinopyroxene). Two types are observed. One consists of a relatively loose collection of prismatic plagioclase ± small equant to skeletal olivine (Fig. F12) that probably forms by aggregation and/or equilibrium growth of phe-

F7. Calcarenite, p. 20.

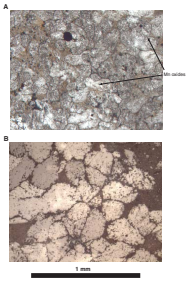

F8. Unaltered glass shard in a calcareous breccia matrix, p. 21.

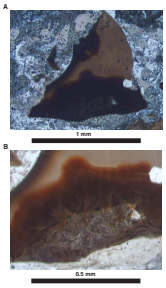

F9. Laminated palagonite clast in calcareous breccia, p. 22.

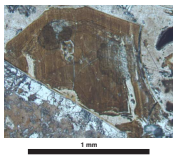

F10. Vermiform palagonite clast in calcareous breccia, p. 23.

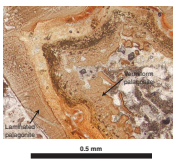

F11. Moderately plagioclase-olivine phyric basalt, p. 24.

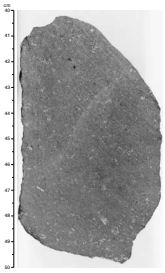

nocrysts during crystallization of the magma. The second glomerocryst type consists of plagioclase partially to totally enclosed in olivine; this type is usually made up of fewer, but generally larger, anhedral crystals. The textural relationship requires that plagioclase crystallized before or together with olivine and that the relationship of the crystals to each other is more typical of cumulate textures (Fig. F13). Glomerocrysts of this type may be xenocrysts incorporated into the magma from a magma chamber. Clinopyroxene phenocrysts were only observed in hand specimen in a single plagioclase + olivine + clinopyroxene glomerocryst in Section 187-1157B-4R-1 (Piece 12). Since clinopyroxene is not observed as a discrete phenocryst phase anywhere in Hole 1157B, it is inferred that the clinopyroxene is part of a xenocrystic glomerocryst.

Groundmass textures range from intersertal to immature sheaf quench morphologies. Mineralogically, the groundmass consists of as much as 50% acicular plagioclase (aspect ratios of up to 30:1; see Fig. F14), ~2% small (<100 µm) equant olivine, and 1%–2% minute (<5 µm) equant opaque minerals. As with the phyric basalts of Hole 1157A, clinopyroxene is usually restricted to quench crystal morphologies intergrown with plagioclase sheaves. However, miarolitic cavities are common and in some cases relatively large—up to 0.7 mm across. Anhedral to subhedral crystals of clinopyroxene and Fe-Ti oxide minerals line or partially fill these cavities, and the crystals are significantly larger than those in the adjacent groundmass (Fig. F15). Alteration tends to be higher in these areas as well (Fig. F16; also see "Hole 1157B," p. 8, in "Alteration"). The miarolitic cavities may explain some of the irregularly shaped pits observed on the cut surfaces of core pieces. Dark brown, quench-textured mesostasis makes up >50% of the rock. Spherical vesicles constitute <1% of the rock and are typically <100 µm in diameter; they are usually unfilled but, in more altered areas, may be filled with calcite (see "Hole 1157B," p. 8, in "Alteration").

Chilled margins are present on 22% of the phyric basalt pieces recovered, and more than half of these margins retain a significant thickness of clear glass (1–6 mm). Similar to the phyric basalts of Hole 1157A, the zone of coalesced spherulites is typically thin (3–4 mm) and composed of relatively small spherulites (~100 µm in diameter). In Sample 187-1157B-2R-1, 48–51 cm, the spherulitic overgrowths on plagioclase are <25 µm wide; overgrowths on olivine crystals are rare to absent (Fig. F17), suggesting very rapid cooling. The abundance of glassy chilled margins recovered and the presence of V-shaped pieces and pieces with curved glassy rinds (Fig. F18) suggest that these basalts are pillow lavas.

Petrography of Sediments

Sediment was not recovered in significant volumes in Hole 1157B. However, small patches a few millimeters to several centimeters across and ≤1 mm thick are common throughout; larger accumulations adhere to the outer surfaces of some pieces or serve as the matrix cementing fragments of glass + palagonite (Fig. F19). In addition, there are strong spatial and compositional relationships between the sediments and some thick veins that crosscut the basalts, suggesting that these represent a continuum of processes ranging from physical infilling to chemical precipitation. For example, interval 187-1157B-3R-2, 109–130 cm (Fig. F20), has a pocket of sediment at one end that is continuous with a composite vein (~3 mm wide) that extends >20 cm along the length of the piece. The vein is typical of those observed throughout Hole 1157B and consists of three materials: (1) pale buff micrite ± clay, (2) darker grayish brown micritic to very finely crystalline sparry cal-

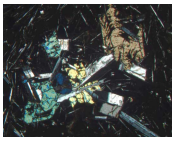

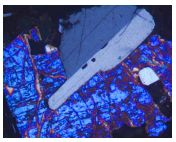

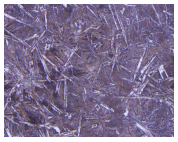

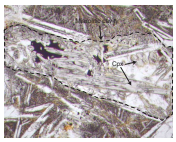

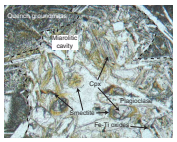

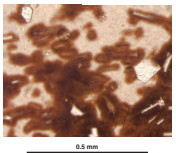

cite, and (3) more coarsely crystalline sparry calcite that crosscuts the first two. These composite veins do not appear to have formed solely by precipitation of calcite and/or clay, since they commonly contain up to 40% small lithic fragments (Fig. F21), similar to those in the breccia matrix in Hole 1157A. The origin of the clasts (i.e., whether they are derived from the adjacent wall rock or are transported from elsewhere) is difficult to assess because most are in an advanced state of alteration and disaggregation (Fig. F22). Many are clearly disaggregated from the adjacent wall rock, but the high abundance of palagonite fragments suggests that many are transported into the pillow interior from its rim. Thus, the veins appear to have a complex origin involving

1. Infill of micritic calcareous sediment ± lithic fragments ± fluids (e.g., Fig. F20),
2. Reaction and dissolution of the wall rock, which replaces primary phases with clays, Fe oxyhydroxides, fibrous amphibole/chlorite?, and/or calcite (Figs. F22, F23),
3. Recrystallization of micritic calcite to very finely crystalline sparry calcite (Fig. F24), and, finally,
4. Generation of thin sparry calcite veins and vug fillings.

The veins and their effect on the alteration of the basalts are described in more detail in "Hole 1157B," p. 8, in "Alteration."

ALTERATION

Hole 1157A

Basalt recovered from Hole 1157A has undergone slight to moderate low-temperature alteration. Along unfilled or calcite-lined fractures, minor alteration has formed halos as wide as 2 mm. Alteration halos within pieces of the basaltic rubble and larger clasts of the basalt-carbonate breccia (Sections 187-1157A-2R-1 and 3R-1) (see "Hole 1157A," p.3 in "Igneous Petrology") extend from 2 to 10 mm inward from outer surfaces and constitute between 5% and 50% of single pieces and clasts (Fig. F6). Smaller clasts of basalt and glass, suspended within the matrix of the breccia, are partially to completely altered (Fig. F25). Outer surfaces of clasts (Section 187-1157A-3R-1) generally have attached Mn oxide concretions, and these surfaces are paralleled by the alteration halos. Some clasts have, however, fractures through the alteration halos, indicating that the alteration occurred before the final phase of brecciation. The majority of pieces in the lower part of the unit (Sections 187-1157A-3R-2 and 4R-1) have highly oxidized, rounded outer margins with coalescing patches of Mn oxide. Pink micrite is occasionally attached to the surfaces of pieces (e.g., Sections 187-1157A-3R-1 [Piece 7] and 4R-1 [Piece 2]).

Within the alteration halos, phenocrysts of olivine are usually partially to completely replaced by Fe oxyhydroxide, but plagioclase is unaltered. The groundmass is partly replaced by a mixture of Fe oxyhydroxide, clay, or calcite. Equant to skeletal hematite is occasionally present within the groundmass calcite. Rare vesicles are empty to partly filled with clay and/or calcite or lined with blue cryptocrystalline silica.

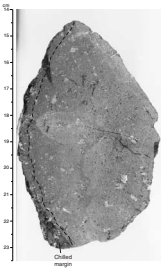

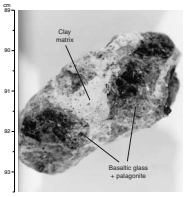

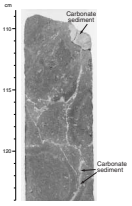

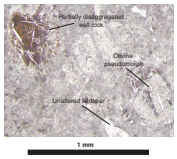

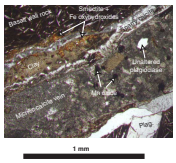

Hole 1157B

Basalt recovered from Hole 1157B represents a single lithologic unit that has been slightly to moderately altered at low temperature. The alteration is generally confined to oxidation halos along fractures, veins, and exterior surfaces (Fig. F26). Many pieces have fresh interiors (e.g., Section 187-1157B-9R-1), but pieces with more pervasive alteration are also present (e.g., Section 8R-1).

Most fractures are unfilled, but some are lined with Mn oxide and/or blue silica and/or clay. Veins (0.1–25 mm wide) filled with carbonate ± Mn oxide ± clay are present in most cores (Figs. F20, F26). Larger veins are filled by micrite sediment and/or sparry calcite. Evidence for transport of micrite sediment into veins comes from micritic sediment pockets attached to the basalt (Fig. F20) with similar micrite in the adjacent veins. Calcite precipitation has also played an important role in the alteration of this core. The sparry calcite may to some extent have been derived from the micrite by recrystallization (Figs. F22, F27). The boundaries between walls and vein fillings are commonly irregular and diffuse. This texture is caused by (1) minute veins/fractures extending into the basalt leading to complete or partial incorporation of small wall fragments into the carbonate (Figs. F28, F29), (2) propagation of fractures around plagioclase microphenocrysts (Fig. F22), and (3) calcite replacement of the wall-rock basalt (Fig. F30).

As much as 40% of vein infill may consist of lithic fragments, including (1) olivine replaced by clay, (2) palagonite (Fig. F31), (3) unaltered to altered plagioclase (Fig. F32), and (4) basalt fragments. All of these clast types are consistent with derivation from the host pillow basalt. Vein boundaries are lined with Fe oxyhydroxide ± clay ± calcite (Fig. F22). Mn oxide dendrites growing into the carbonate from the altered basalt wall, as well as minute red spots of Fe oxides, are commonly present.

Calcite veins are usually surrounded by symmetric alteration halos as wide as ~25 mm, generally ~10 mm (Fig. F26). Within the alteration halos in the upper part of the unit (Cores 187-1157B-2R through 4R), 100% of olivine phenocrysts are completely replaced by Fe oxyhydroxide; elsewhere, 0%–40% of olivine is altered to Fe oxyhydroxide or white clay. Within alteration halos in the lower part of the unit (Sections 1157B-5R-1 through 9R-1), 30%–100% of olivine phenocrysts are partly to completely replaced by Fe oxyhydroxide ± green-yellow clay or calcite (Fig. F33). Plagioclase phenocrysts are usually unaltered throughout. The groundmass usually shows patchy replacement of olivine and mesostasis by yellow-brown and/or olive-green clay ± Fe oxyhydroxide and rarely calcite within the halos. In Section 187-1157B-8R-2, however, the alteration tends to be pervasive. Vesicles are empty to variably filled with clay or lined with Fe oxyhydroxide or blue silica.

The outer parts of glassy pillow margins are altered in variable degree to yellowish brown to orange palagonite. No alteration halos are observed adjacent to the glassy margins.

MICROBIOLOGY

At Site 1157, four rock samples were collected to characterize the microbial community inhabiting this environment (Table T2). Breccia fragments (Sample 187-1157A-3R-1 [Piece 20, 120–123 cm]) and pillow basalt fragments, composed of partially altered glass rinds and crystal-

F23. Boundary of a partially recrystallized micritic vein, p. 36.

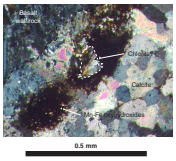

F24. Partially recrystallized calcite vein, p. 37.

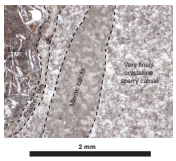

F25. Partially altered basalt glass shard in calcareous sediment, p. 38.

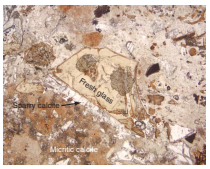

F26. Calcite veins dissecting basalt, p. 39.

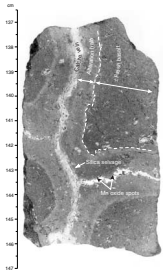

F27. Boundary of micritic vein partially recrystallized to very finely crystalline sparry calcite, p. 40.

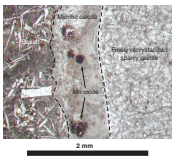

F28. Highly altered basalt clast within micritic calcite vein, p. 41.

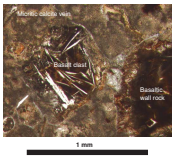

line basalt (Samples 187-1157B-4R-2 [Piece 10, 68–72 cm] and 187-1157B-8R-1 [Piece 6A, 39–46 cm]), or crystalline basalt only (Sample 187-1157B-2R-1 [Piece 7, 44–47 cm]) were sampled as soon as the core liners were split. To sterilize them, the outer surfaces of the rocks were quickly flamed with an acetylene torch. Enrichment cultures and samples for DNA analysis and electron microscope studies were prepared (see **"Igneous Rocks,"** p. 7, in "Microbiology" in the "Explanatory Notes" chapter).

Fluorescent microsphere tests were carried out for three rock cores to evaluate the extent of contamination caused by drilling fluid (Table **T2**) (see **"Tracer Test,"** p. 9, in "Microbiology" in the "Explanatory Notes" chapter). Pieces of rock from each core were rinsed in nanopure water, and then the water was filtered. Thin sections were used to examine the extent of contamination inside the samples. Filters and thin sections were examined under a fluorescence microscope for the presence of microspheres. Microspheres were detected on all three filters; in the thin sections microspheres were located both inside fractures and on thin-section surfaces. The microspheres on the polished surfaces were always found close to fractures or to thin-section (i.e., piece) margins and may have been relocated by polishing. Sixty microspheres were observed in thin sections from Core 187-1157A-2R, 14 from Core 187-1157B-2R, and 96 from Core 187-1157B-8R.

STRUCTURAL GEOLOGY

Hole 1157A

In basalt from Hole 1157A, the fracture + vein density ranges from 3.6 to 25.5/m and averages 13.6/m (Fig. **F34**). The vein density ranges from 0 to 4.3/m and averages 2.3/m. The calculated volume percent of veins ranges from 0 to 0.05 and averages 0.02. As with cores from Site 1156, fracture + vein density is significantly higher in Core 187-1157A-4R, which is exclusively basalt fragments, as compared with the upper cores from this hole, which are from a basaltic breccia.

Hole 1157B

Cores from Hole 1157B have more fractures and veins than those from Hole 1157A. The fracture + vein density in basalts from Hole 1157B ranges from 12.0 to 32.3/m and averages 21.3/m (Fig. **F34**). The vein density ranges from 0 to 19.7 /m and averages 9.0/m. The calculated volume percent of veins ranges from 0 to 1.78 and averages 0.69.

SITE GEOPHYSICS

Site 1157 was located based on 1997 SCS site survey data and confirmed by a short 3.5-kHz PDR and SCS presite survey from the *JOIDES Resolution* (JR). Onboard instrumentation included a precision echo sounder, gyrocompass, seismic system, and GPS receivers.

Seismic Reflection Profiling

Site selection for Site 1157 was based on a SCS survey conducted during *R/V Melville* cruise Sojourner 5 in 1997. A 1-hr SCS and 3.5-kHz PDR

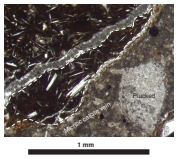

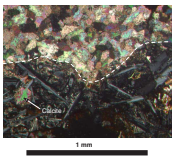

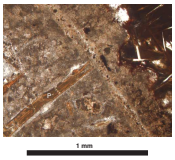

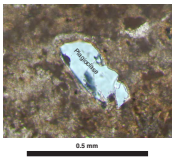

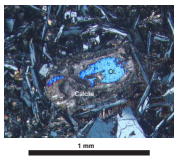

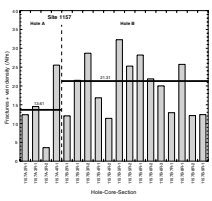

survey was conducted on the approach to Site 1157 (JR SCS line S6; Fig. F35) to ensure the correct site location. The ship's average speed was 5.5 kt during the survey. The water gun was triggered at a shot interval of 12 s, equivalent to ~34 m at 5.5 kt. Data acquisition and processing parameters are described in "Underway Geophysics," p. 10, in the "Explanatory Notes" chapter. Survey line S6 was conducted on a heading of 115°and roughly perpendicular to the site survey line. The final position of Site 1157 was chosen ~1.85 km east of the prospectus site AAD-28a (Fig. F35), where sediment cover appears to be thinner. We marked the position of Hole 1157A near seismic shotpoint 157 of line S6, where the water depth is 5080.4 m (see Fig. F36). Although there are significant out-of-plane reflectors, the sediment cover (Fig. F36) extends from 6.83 s to at least 6.98 s in two-way traveltime, equivalent to a minimum of 150 m of sediment. Hole 1157A penetrated 200 m of sediment before basement was reached, whereas Hole 1157B, about 200 m west of Hole 1157A, encountered only ~136 m of sediment, indicating significant basement roughness.

F35. Track chart of the JR SCS survey line S6, p. 48.

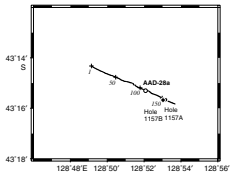

F36. SCS profile of line S6 from shotpoints 1 to 170, p. 49.

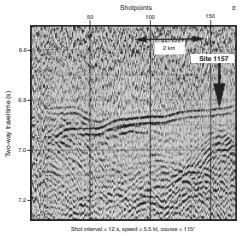

SEDIMENTS

A full wash barrel (Core 187-1157A-1W; 0.0–200.0 mbsf) was recovered from Hole 1157A. Most of the core is highly to moderately drilling disturbed but is characterized by intervals of contrasting color, from dark to medium brown siliceous clay (Fig. F37). Contacts between the different colored intervals are deformed; some are diffuse, and longer intervals of one color commonly contain wispy intervals of the other. In two cores (187-1157A-2W and 3W), there are 50-cm-thick intervals where the color change is gradational from dark to light and light to dark, respectively. The changes are manifested as increasing abundances of thin intervals of one hue within the other. In Section 187-1157A-1W-1, a distinct, originally planar, deformed contact dips ~70° across the cut face of the core. In Section 187-1157A-1W-5, an irregular, steeply dipping (~85°) contact between light brown and medium to dark brown clay. Rare light gray intervals occur sporadically throughout the core.

F37. Color variation in Core 187-1157A-1W, p. 50.

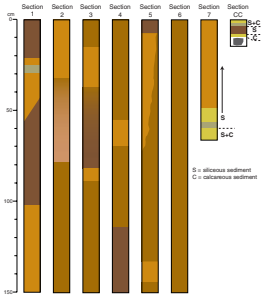

Toward the bottom of Section 187-1157A-1W-7 is a distinct color change to much lighter brown silty clay, but carbonate is only detectable in the lowermost 6 cm of the section (see Fig. F37), where it effervesces slightly with dilute HCl (~5%–10%). Carbonate-bearing clay is also present in the top of the core-catcher section. It is underlain by a sharp contact with dark brown siliceous clay that lacks a calcareous component. Below the dark brown siliceous clay is a 2-cm-thick interval of calcareous clay that effervesces violently with dilute HCl.

Five smear slides were prepared. In the predominant dark brown and medium brown clay, siliceous microfossil fragments are abundant. Honeycomb-textured fragments as large as 50 µm across have circular void spaces from 1 to 20 µm in diameter. Colorless acicular to semicircular spines are also abundant, as are elongate elliptical microfossils with subparallel, axis-perpendicular septa. Rare 4- to 6-µm rounded, translucent, brown fragments of volcanic glass and colorless crystal shards comprise <1% of the sediment. The only apparent differences among the dark brown, the medium brown, and the rare light gray clay intervals are slight color differences in aggregated clay particles. A smear slide from the interval at the base of Section 187-1157A-1W-7 contains a mixed assemblage of siliceous and calcareous microfossils and rare

trace components as in the overlying sediment. The lowermost calcareous ooze contains abundant calcareous microfossils; no siliceous microfossils were recognized.

GEOCHEMISTRY

Introduction

Site 1157 is located on ~22-Ma crust formed within Zone A ~230 km south of Site 1153 (~23 Ma). Two holes were drilled, and in each hole the rocks were assigned to a single lithologic unit. Two whole-rock samples from Hole 1157A and two from Hole 1157B were analyzed for major and trace elements by inductively coupled plasma–atomic emission spectrometry (ICP-AES) and X-ray fluorescence (XRF). One glass sample from each hole was analyzed by ICP-AES (Table T3). The ICP-AES and XRF results for whole rocks agree well, although Cr and Ni remain problematic.

T3. Compositions of basalts, Site 1157, p. 56.

Hole 1157A

Hole 1157A recovered mixed aphyric and moderately plagioclase-olivine phyric pillow basalt rubble as well as basalt-carbonate breccia. Samples analyzed from this hole include an aphyric whole rock, a plagioclase-olivine phyric whole rock, and a glass rind from a basalt clast recovered in the core catcher of the wash barrel. MgO contents range from ~7.0 to 8.5 wt%; the aphyric sample is the most evolved, and the glass is the least evolved (Fig. F38). The three samples generally define linear trends on most MgO variation diagrams, consistent with low-pressure crystal fractionation. However, Na_2O varies orthogonally to a simple crystal fractionation trend which can only be explained by loss of MgO and/or mobility of Na_2O during alteration of the whole-rock samples.

F38. Major element compositions of basalts from Holes 1157A and 1157B vs. MgO, p. 51.

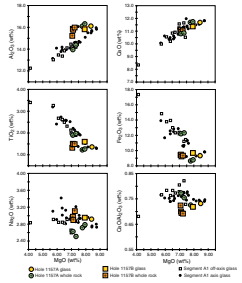

Hole 1157B

Hole 1157B recovered moderately plagioclase-olivine phyric pillow basalt. The samples from 1157B show a similar range of MgO contents (i.e., ~7 to 8 wt%), and the glass composition lies along the same low-pressure crystal fractionation trends as the samples from Site 1157A, but the whole-rock data have significantly lower TiO_2 and CaO/Al_2O_3 values and higher Al_2O_3 and Cr at a given MgO content. As observed for previous sites, the glass is nearly 1.0 wt% higher in MgO content than are the associated whole rocks from this core. However, most other major and trace constituents are similar to the glass composition; only Ni is significantly different.

F39. Trace element compositions of basalts from Holes 1157A and 1157B vs. MgO, p. 52.

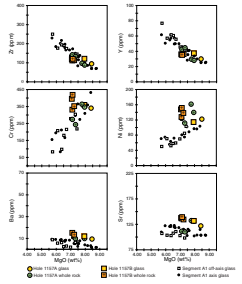

Temporal Variations

Together, the Site 1157 basalts are generally a coherent group, except that whole-rock Sample 187-1157A-2R-1, 86–90 cm, is low in Sr relative to the rest of the samples. Compared to 0- to 7-Ma Zone A basalts, most Site 1157 lavas have similar CaO, Zr, Y, and Cr contents, but lower Fe_2O_3, CaO/Al_2O_3, and TiO_2 and higher Al_2O_3, Ni, Ba, and Sr (Figs. F38, F39). Low Fe_2O_3, CaO/Al_2O_3, and TiO_2 values and high Al_2O_3, Ni, Ba,

and Sr are characteristics typical of lavas dredged within the AAD and are traits uncommon in Zone A.

Comparison of Zone A axis and off-axis basalts with Site 1157 basalts reveals an interesting temporal variability in Ba, Sr, and CaO/Al_2O_3. The three groups define parallel trends with decreasing MgO, suggesting variations in source parameters for this part of the Southeast Indian Ridge (SEIR). For instance, if high CaO/Al_2O_3 content indicates a high degree of melting (Falloon and Green, 1987; Klein and Langmuir, 1987), then the Site 1157 lavas were by formed by lower degrees of melting than the axis and off-axis Zone A lavas, which formed by intermediate and high degrees of melting, respectively. Site 1157 basalts appear to have been produced during a particularly lean magmatic period. Variations in Ba and Sr are consistent with this melting scenario, but the low Na_2O content for Site 1157 lavas is not. We speculate that such variations in melting are caused by the repeated arrival and demise of propagating rift–dying rift pairs along this section of the SEIR. Site 1157 lava could have erupted during a waning magmatic cycle associated with a dying rift.

In addition, major and trace element variations at Site 1157 are quite different from those at Site 1153 (see **"Geochemistry,"** p. 6, in the "Site 1153" chapter), the most interesting contrasts being that Fe_2O_3, TiO_2, Zr, and Y contents at Site 1153 are relatively high. These compositional variations indicate a continual evolution of mantle conditions along the eastern border of the AAD.

Mantle Domain

The Zr/Ba systematics of Site 1157 basalts indicate that Indian- to Transitional-Pacific–type mantle was present east of the AAD at ~22 Ma (Fig. **F40A**). The Na_2O/TiO_2 values, relative to the overall variation for Leg 187 basalts, also indicate an Indian-type source (Fig. **F40B**). An interesting aspect of these diagrams is shown by whole-rock Sample 187-1157A 2R-1, 86–90 cm. This whole-rock sample appears (Fig. **F40B**) to be of Pacific type, and it consistently lies along the fractionation trend defined by Segment A1 lavas. All other Site 1157 basalts have Indian-type characteristics, like the associated glasses. The significance of this sample will not be known until we better understand the Ba systematics of the whole-rock samples and can corroborate these conclusions with isotopic data.

F40. Variations of Zr/Ba vs. Ba and Na_2O/TiO_2 vs. MgO for Hole 1157A and Hole 1157B basaltic glass and whole rock, p. 53.

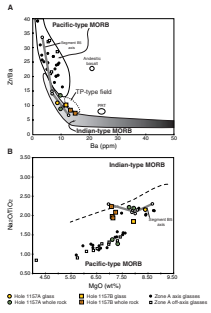

REFERENCES

Falloon, T.J., and Green, D.H., 1988. Anhydrous partial melting of peridotite from 8 to 35 kb and the petrogenesis of MORB. *J. Petrol., Spec. Lithosphere Iss.,* 379–414.

Klein, E.M., and Langmuir, C.H., 1987. Global correlations of ocean ridge basalt chemistry with axial depth and crustal thickness. *J. Geophys. Res.,* 92:8089–8115.

Figure F1. Photograph of basalt breccia Section 187-1157A-3R-1 (Piece 6), which contains clasts of both aphyric and plagioclase-olivine phyric basalt. Chilled margins are evident on both clasts (i.e., the darker glassy area of the phyric basalt and the spherulitic chilled margin of the aphyric basalt emphasized in the lighter alteration halo).

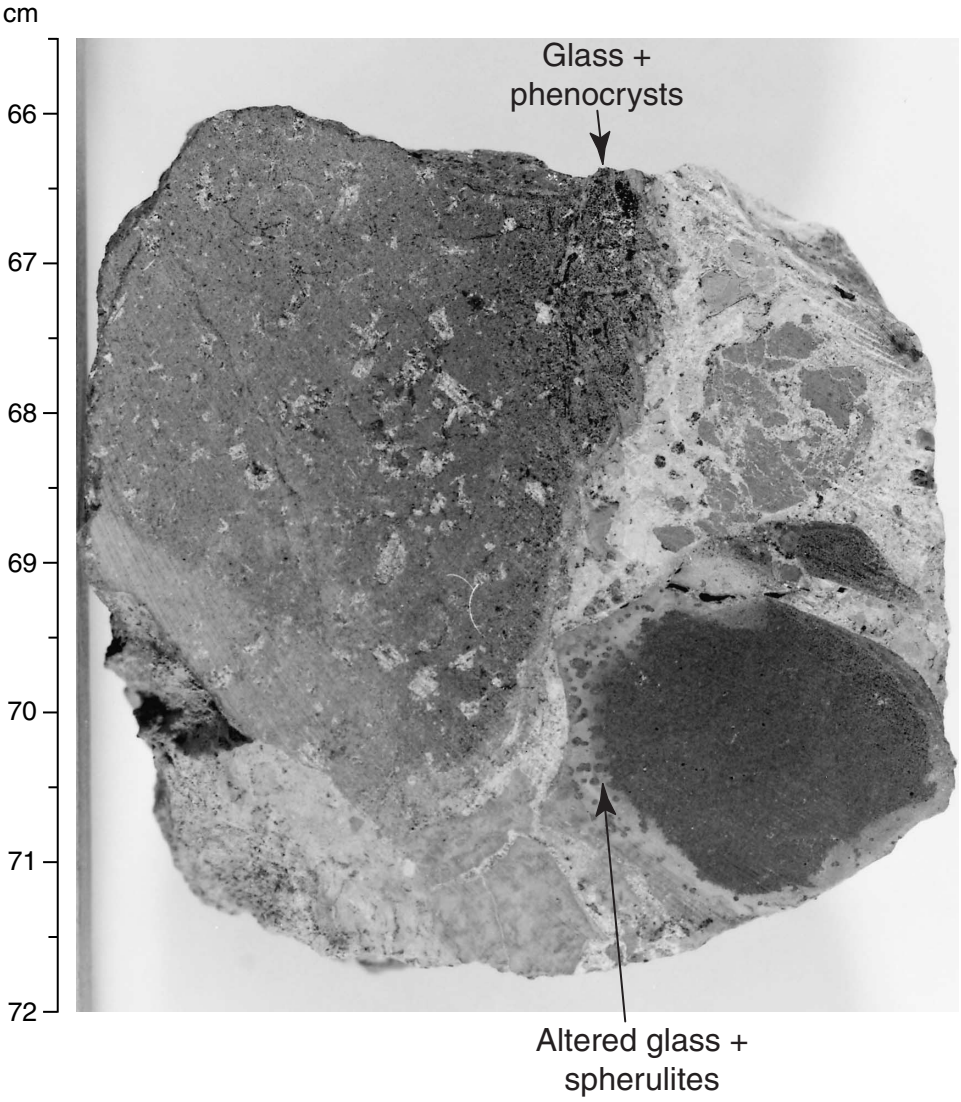

Figure F2. Photomicrograph, with crossed polars, of Sample 187-1157A-3R-2, 19–22 cm (see "Site 1157 Thin Sections," p. 23), showing euhedral clinopyroxene growth into a miarolitic cavity, now filled with calcite.

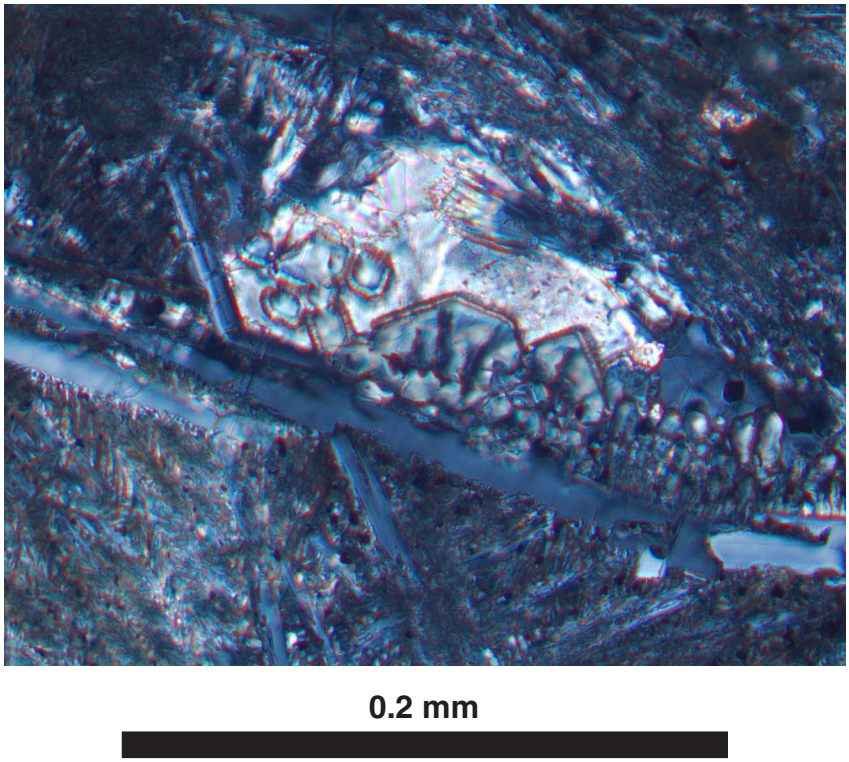

Figure F3. Photomicrograph, with crossed polars, of Sample 187-1157A-2R-1, 86–90 cm (see **"Site 1157 Thin Sections,"** p. 22), showing skeletal olivine microphenocrysts and plagioclase sheaf quench texture in aphyric basalt; note the small (<50 µm) groundmass olivines.

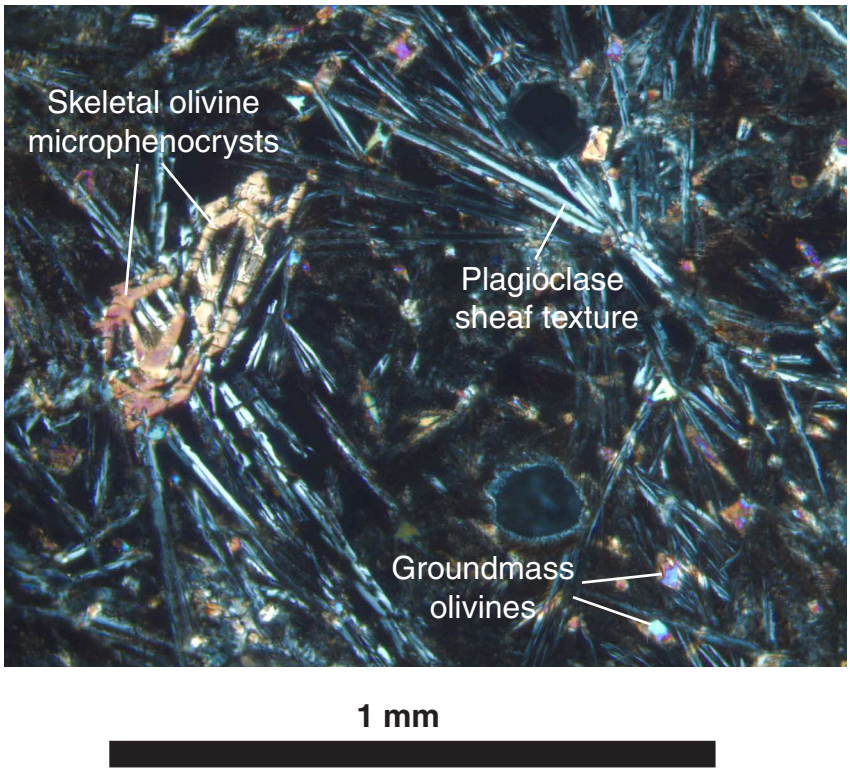

Figure F4. Photograph of interval 187-1157A-3R-1, 124–132 cm, showing a wide spherulitic chilled margin (between 124 and 128 cm) composed of spherulites as large as 2 mm.

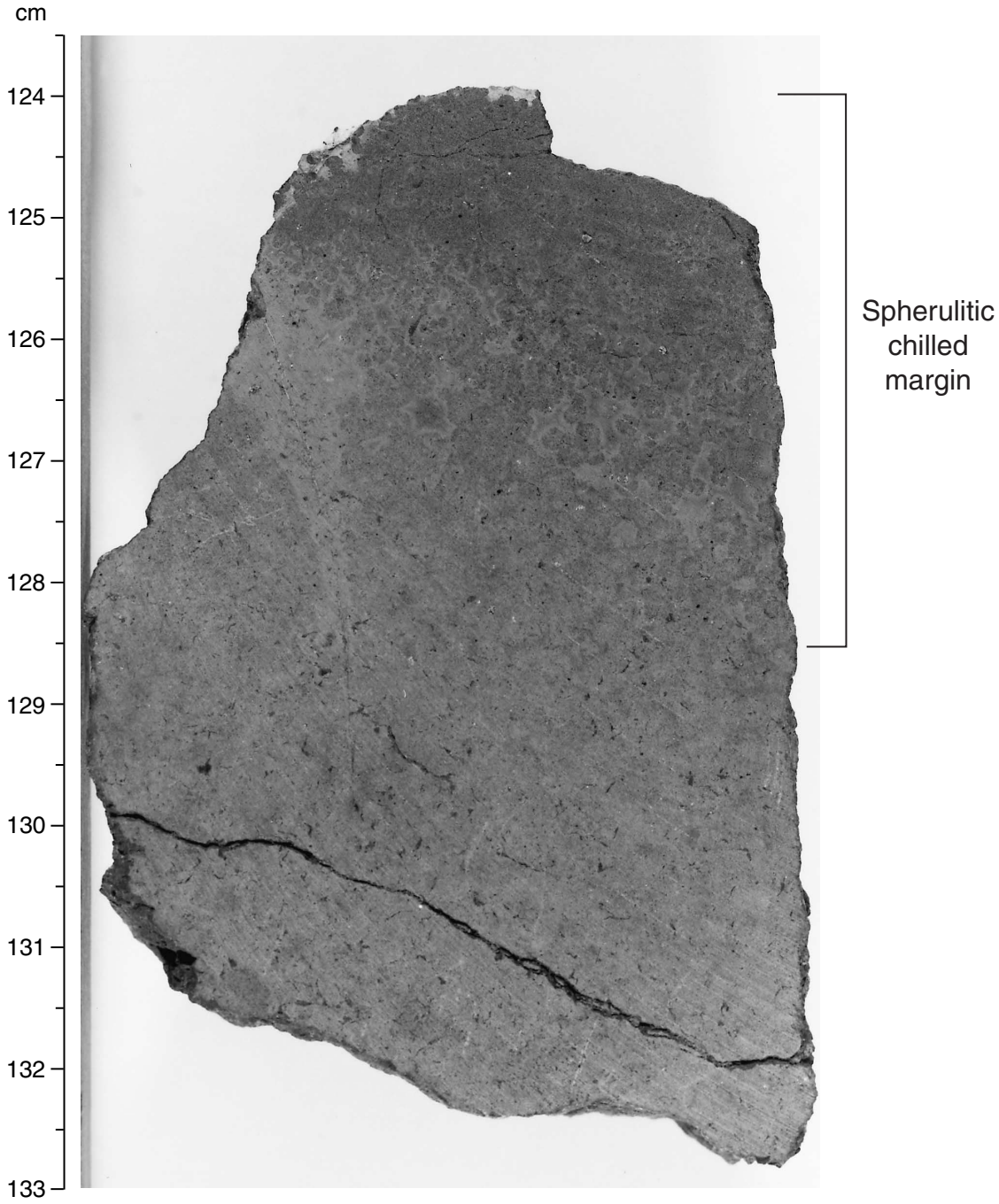

Figure F5. Photograph of interval 187-1157A-2R-1, 33–40 cm, showing calcarenite sediment partially enclosing a plagioclase-olivine phyric basalt clast.

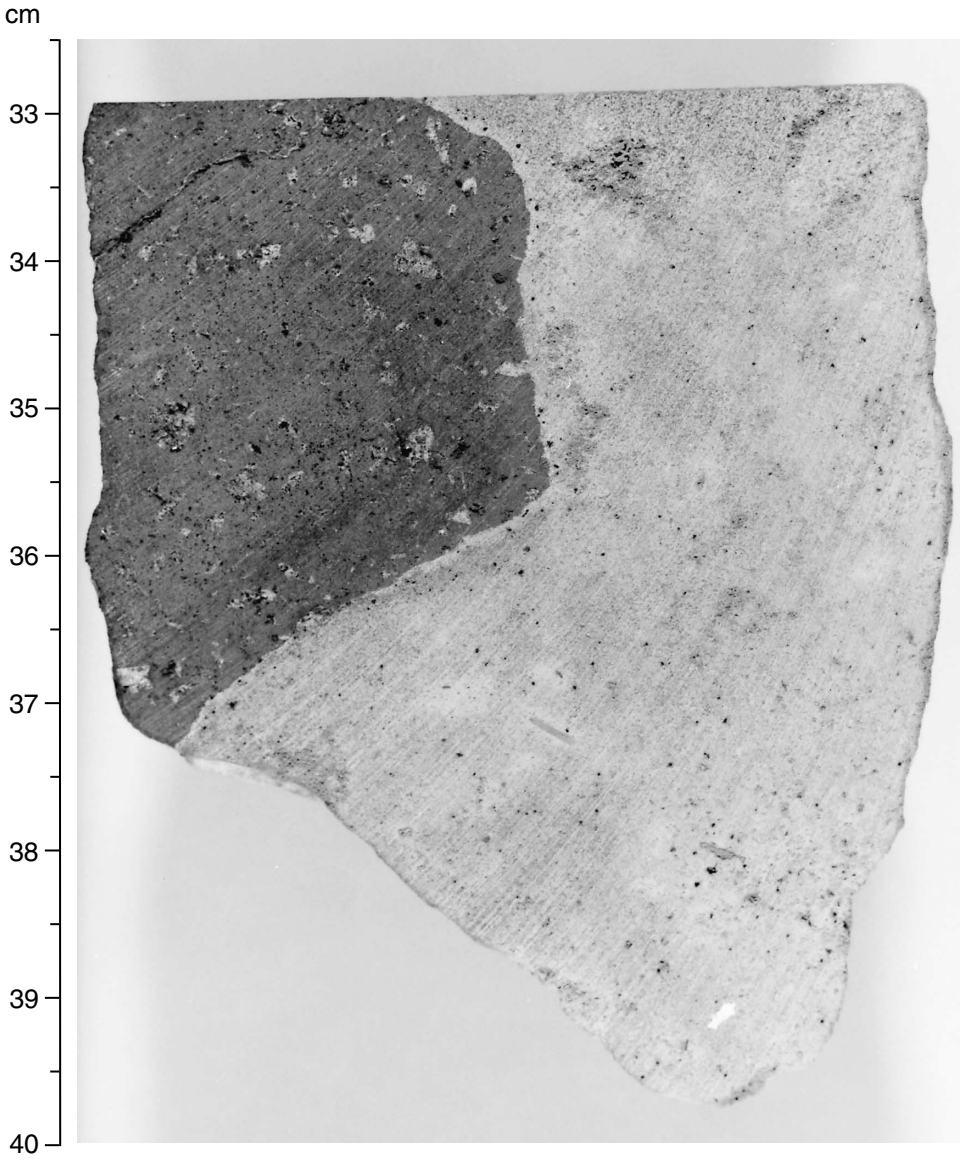

Figure F6. Photograph of interval 187-1157A-3R-1, 73–82 cm, showing basalt breccia with lithic-rich calcareous sediment matrix composed of clay, micritic calcite, and sparry calcite. Large clast between 74 and 76 cm has a spherulitic chilled margin and a relatively fresh core surrounded by a lighter colored alteration halo.

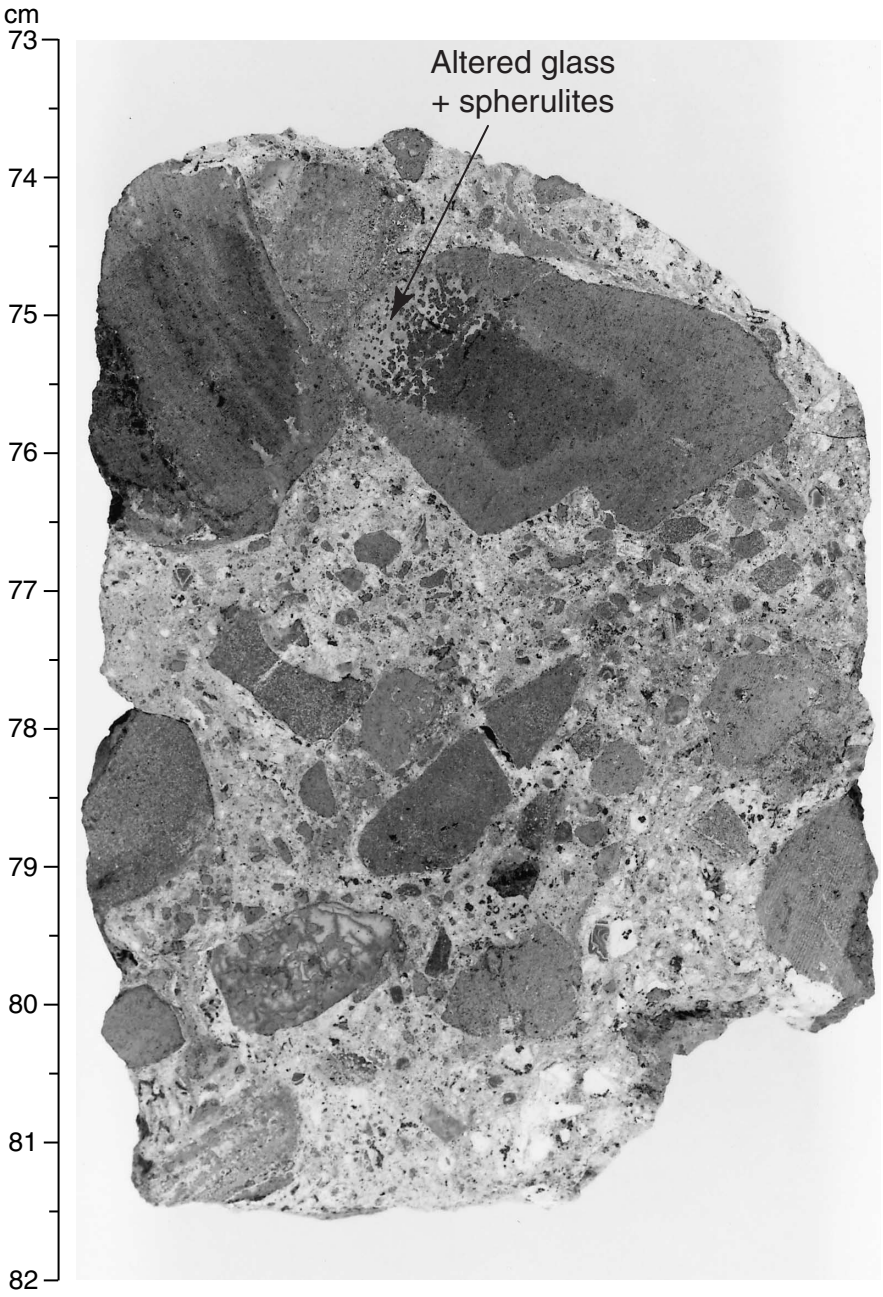

Figure F7. A. Photomicrograph in plane-polarized light of Sample 187-1157A-2R-1, 30–33 cm (see "Site 1157 Thin Sections," p. 20), showing calcarenite sediment, which occurs adhering to a basalt breccia clast (not shown). Note the round to elongate shapes of the crystals and the presence of small to medium-sized Mn oxide concretions throughout. **B.** Photomicrograph of the same sample in reflected light showing round to elongate shapes of calcite crystals (bright areas) surrounded by interstitial clay (darker areas).

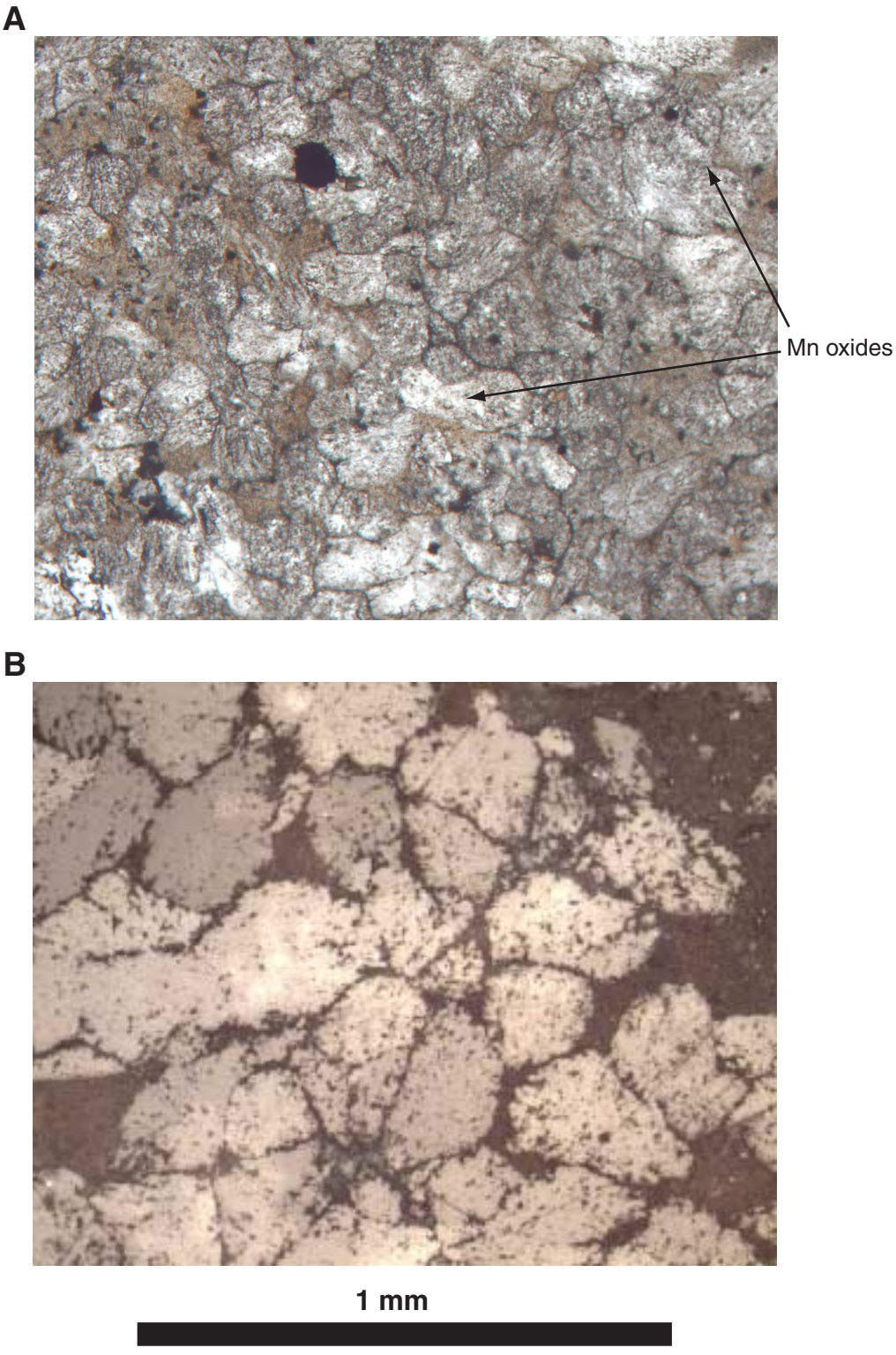

Figure F8. A. Photomicrograph in plane-polarized light of Sample 187-1157A-2R-1, 30–33 cm (see "Site 1157 Thin Sections," p. 20), showing an unaltered glass shard with quench crystals occurring as a clast in calcareous breccia matrix. **B.** Photomicrograph in plane-polarized light detailing the quench crystals in the glass shard pictured in A.

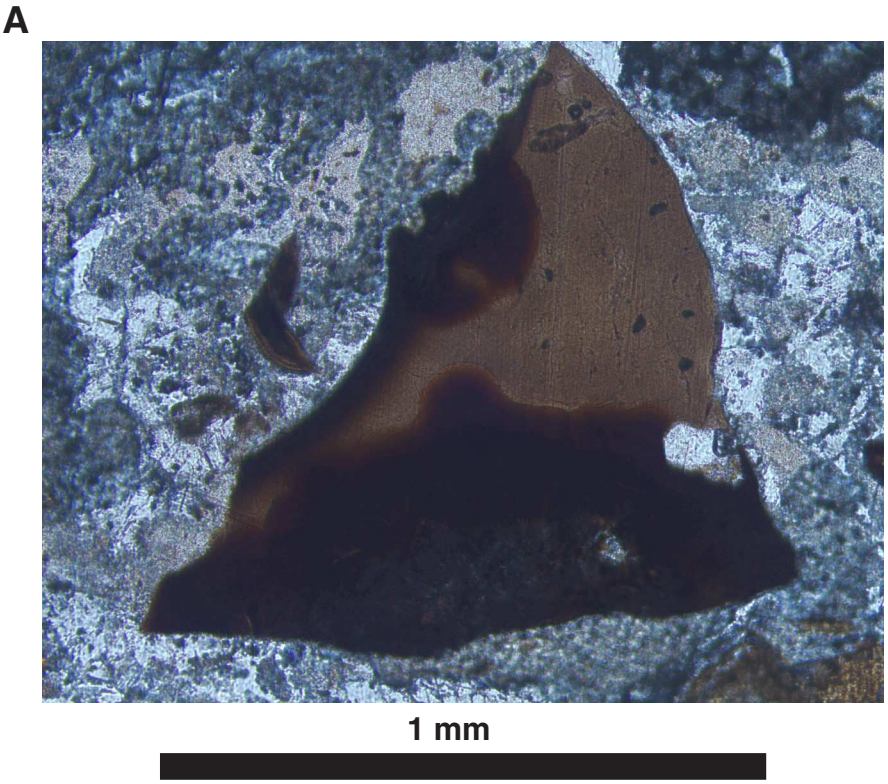

Figure F9. Photomicrograph in plane-polarized light of Sample 187-1157A-2R-1, 30–33 cm (see **"Site 1157 Thin Sections,"** p. 20), showing laminated texture of a palagonite clast in calcareous breccia matrix.

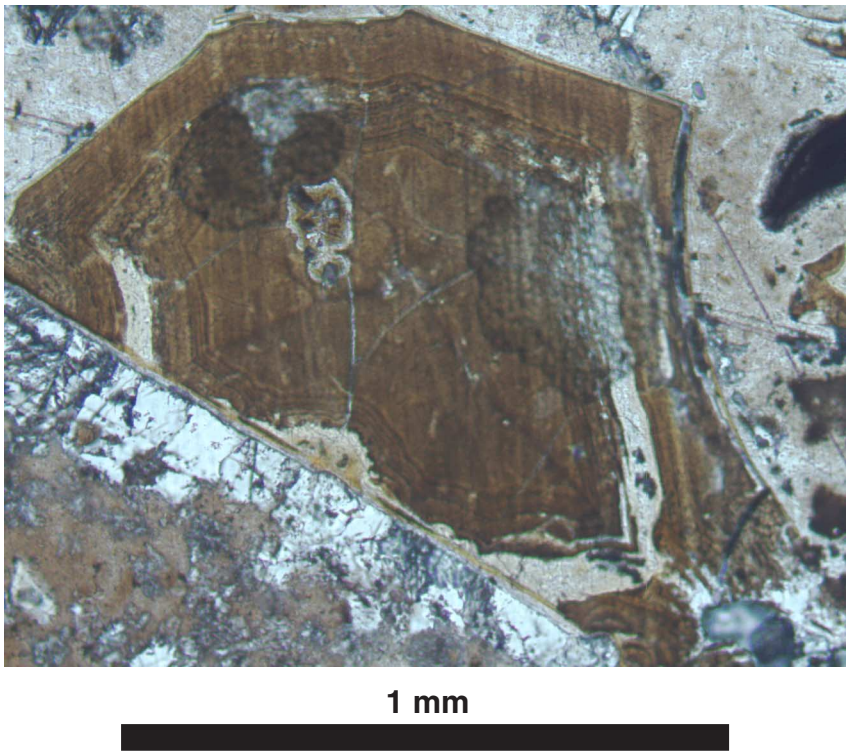

Figure F10. Photomicrograph in plane-polarized light of Sample 187-1157A-2R-1, 30–33 cm (see "Site 1157 Thin Sections," p. 20), showing vermiform texture of a palagonite clast in calcareous breccia matrix.

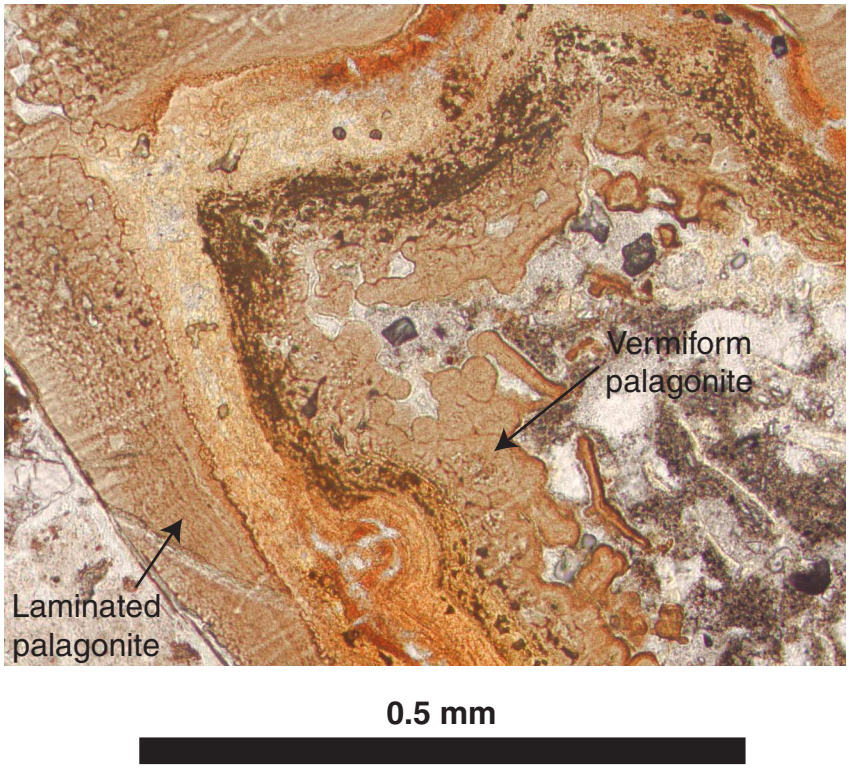

Figure F11. Photograph of interval 187-1157B-6R-1, 40–50 cm, showing a moderately plagioclase-olivine phyric basalt typical of Unit 1.

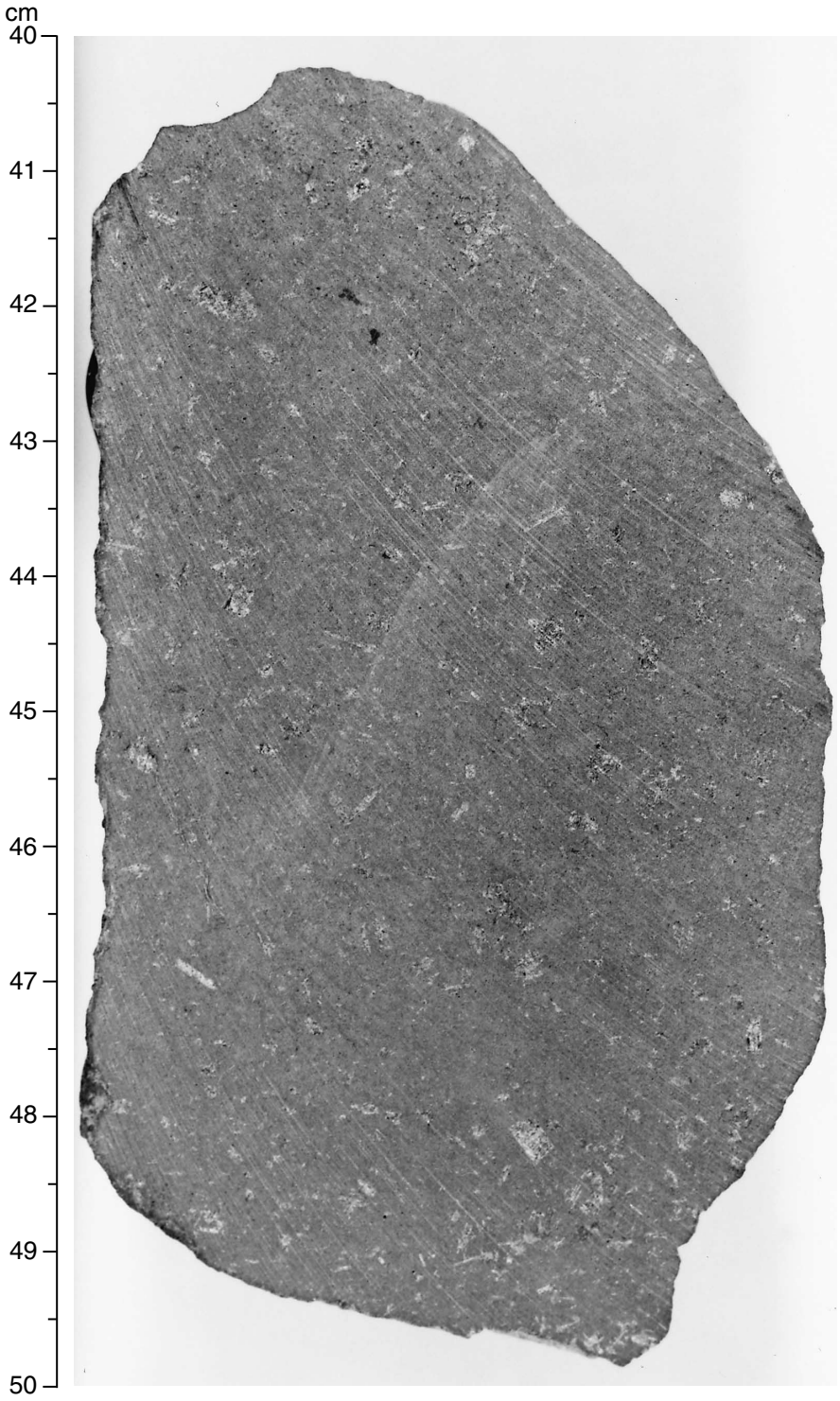

Figure F12. Photomicrograph, with crossed polars, of Sample 187-1157B-6R-1, 43–47 cm (see "Site 1157 Thin Sections," p. 29), showing a plagioclase + olivine glomerocryst consisting of intergrown prismatic plagioclase and skeletal olivine phenocrysts.

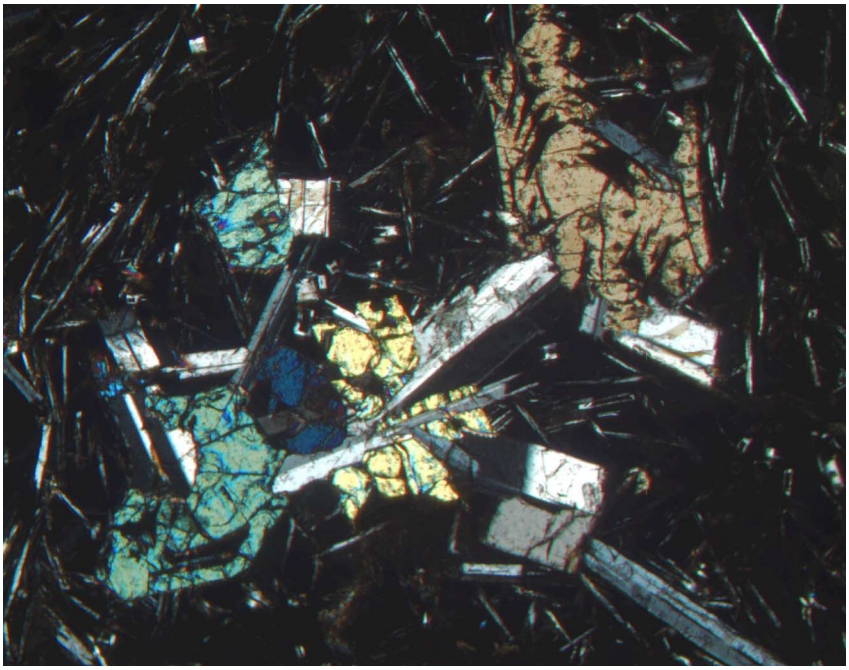

Figure F13. Photomicrograph, with crossed polars, of Sample 187-1157B-2R-1, 48–51 cm (see "Site 1157 Thin Sections," p. 24), showing plagioclase partially enclosed in olivine.

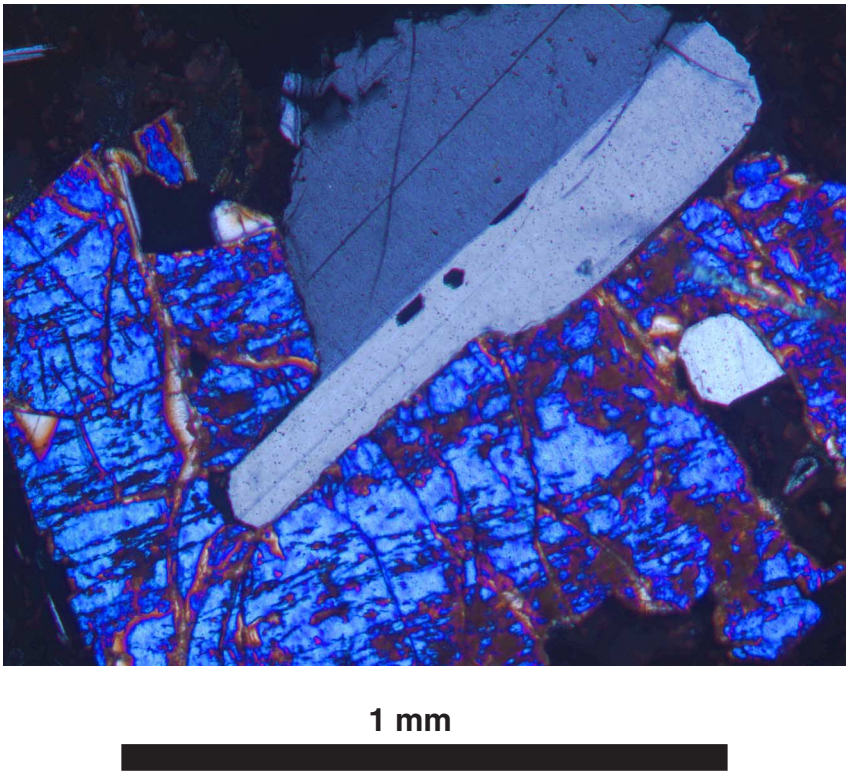

Figure F14. Photomicrograph in plane-polarized light of Sample 187-1157B-3R-1, 62–67 cm (see "Site 1157 Thin Sections," p. 25), showing typical quench groundmass texture of moderately plagioclase-olivine phyric basalt, Unit 1. Note the range of acicular to skeletal plagioclase groundmass morphologies.

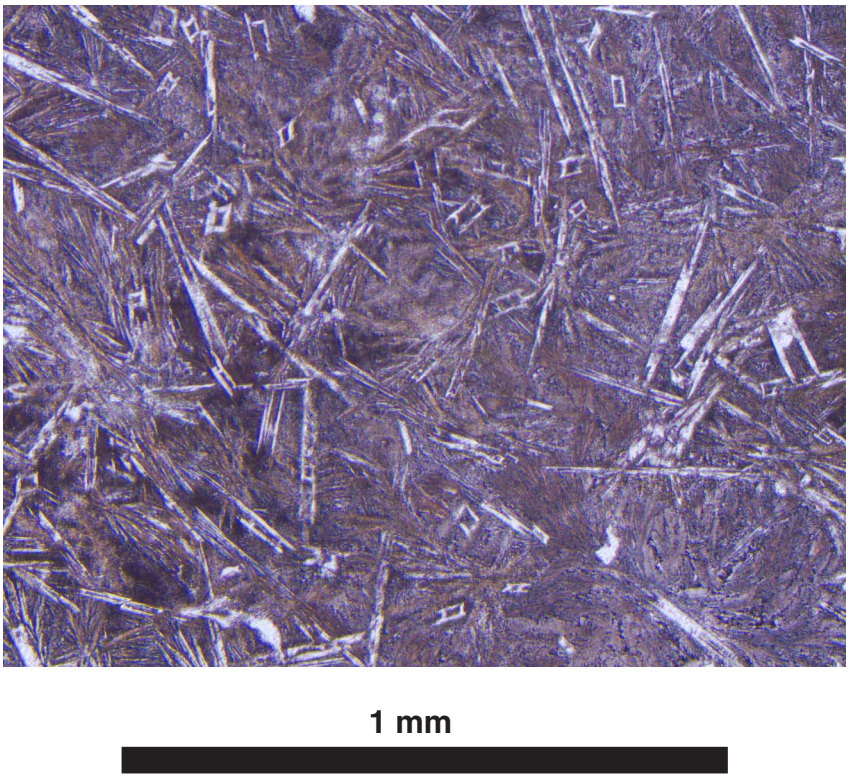

Figure F15. Photomicrograph in plane-polarized light of Sample 187-1157B-3R-1, 97–101 cm (see "Site 1157 Thin Sections," p. 26), showing a miarolitic cavity (dashed outline) with enlarged Fe-Ti oxides and elongate clinopyroxene (Cpx = clinopyroxene, long pale brown minerals) compared to more typical quench groundmass textures visible in the adjacent areas.

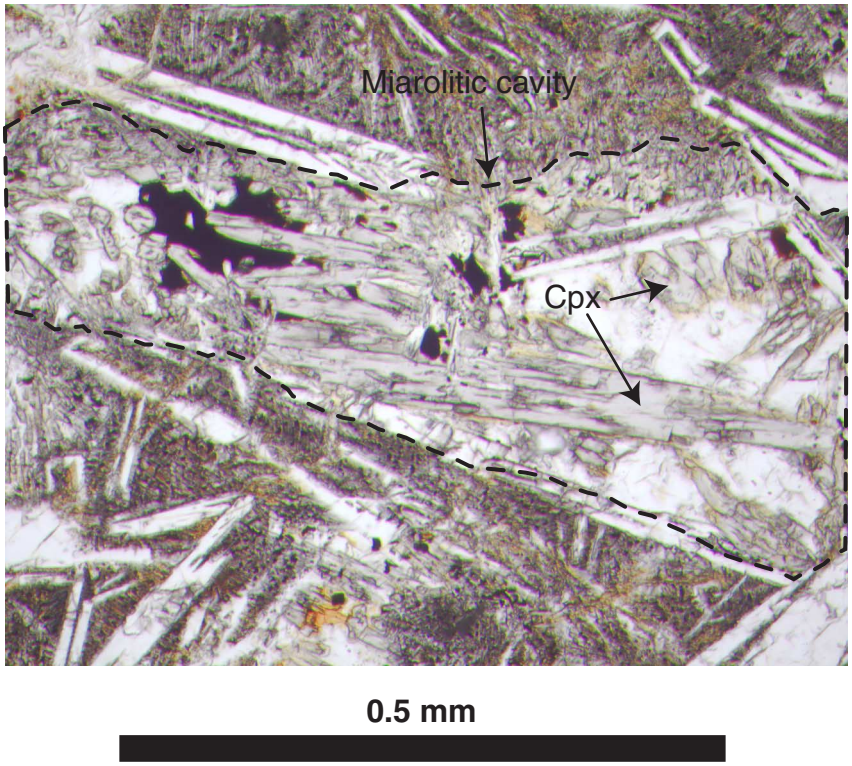

Figure F16. Photomicrograph in plane-polarized light of Sample 187-1157B-3R-1, 97–101 cm (see **"Site 1157 Thin Sections,"** p. 26), showing a miarolitic cavity (dashed outline). Notice the higher degree of alteration to Fe oxyhydroxides and clay in the cavity area relative to groundmass away from the cavity (better shown in Fig. **F15,** p. 28). Cpx = clinopyroxene.

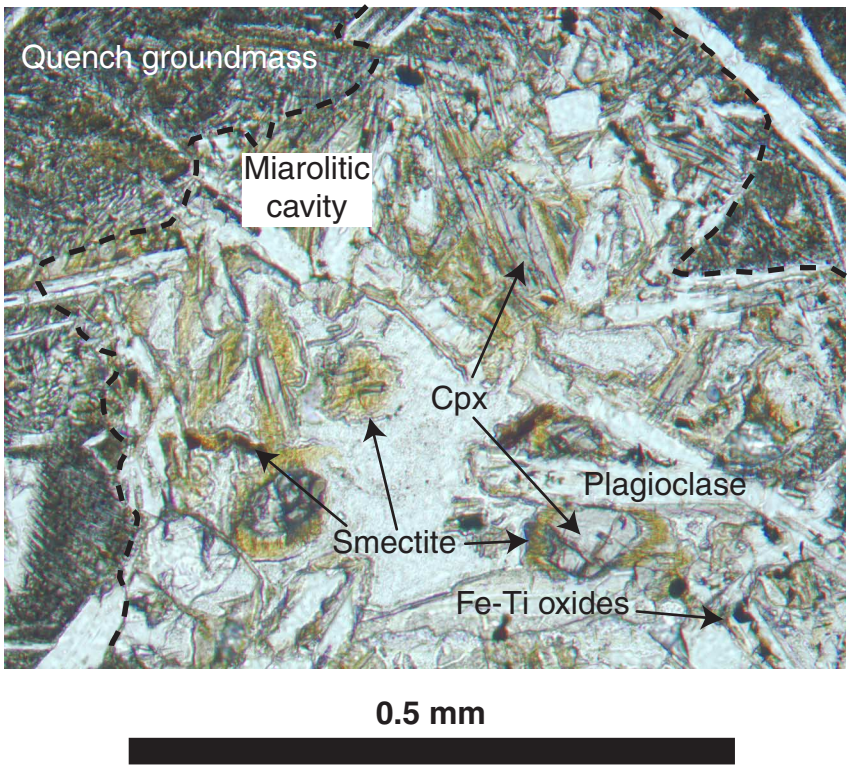

Figure F17. Photomicrograph in plane-polarized light of Sample 187-1157B-2R-1, 48–51 cm (see "Site 1157 Thin Sections," p. 24), showing part of a glassy chilled margin with small quench overgrowths (dark brown material) on plagioclase and rare to absent overgrowths on olivine.

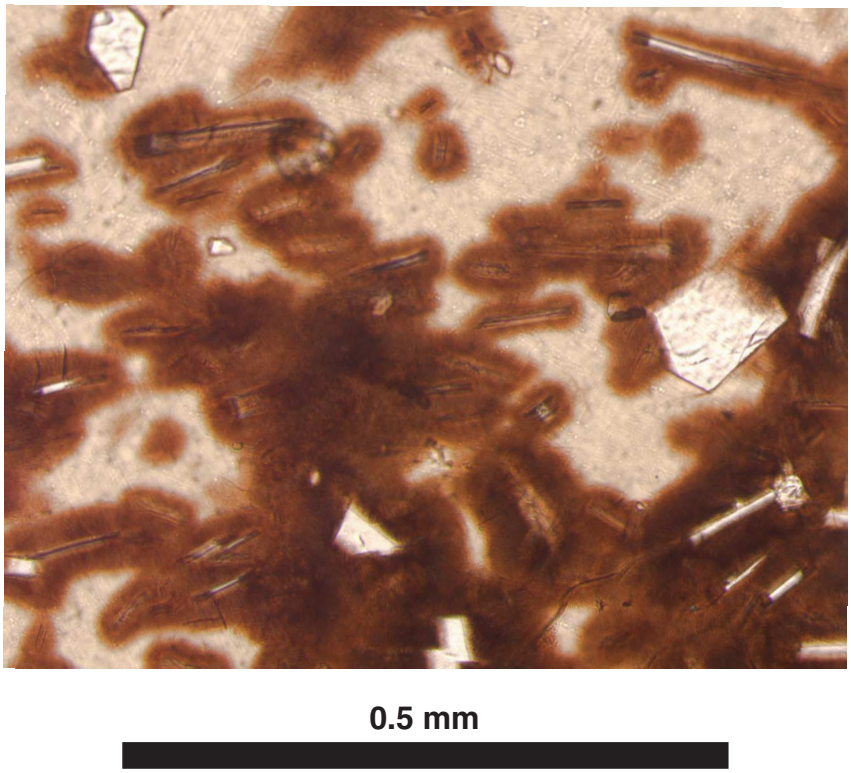

Figure F18. Photograph of interval 187-1157B-3R-1, 15–23 cm, showing a curved chilled margin on plagioclase-olivine phyric basalt indicative of a pillow lava origin.

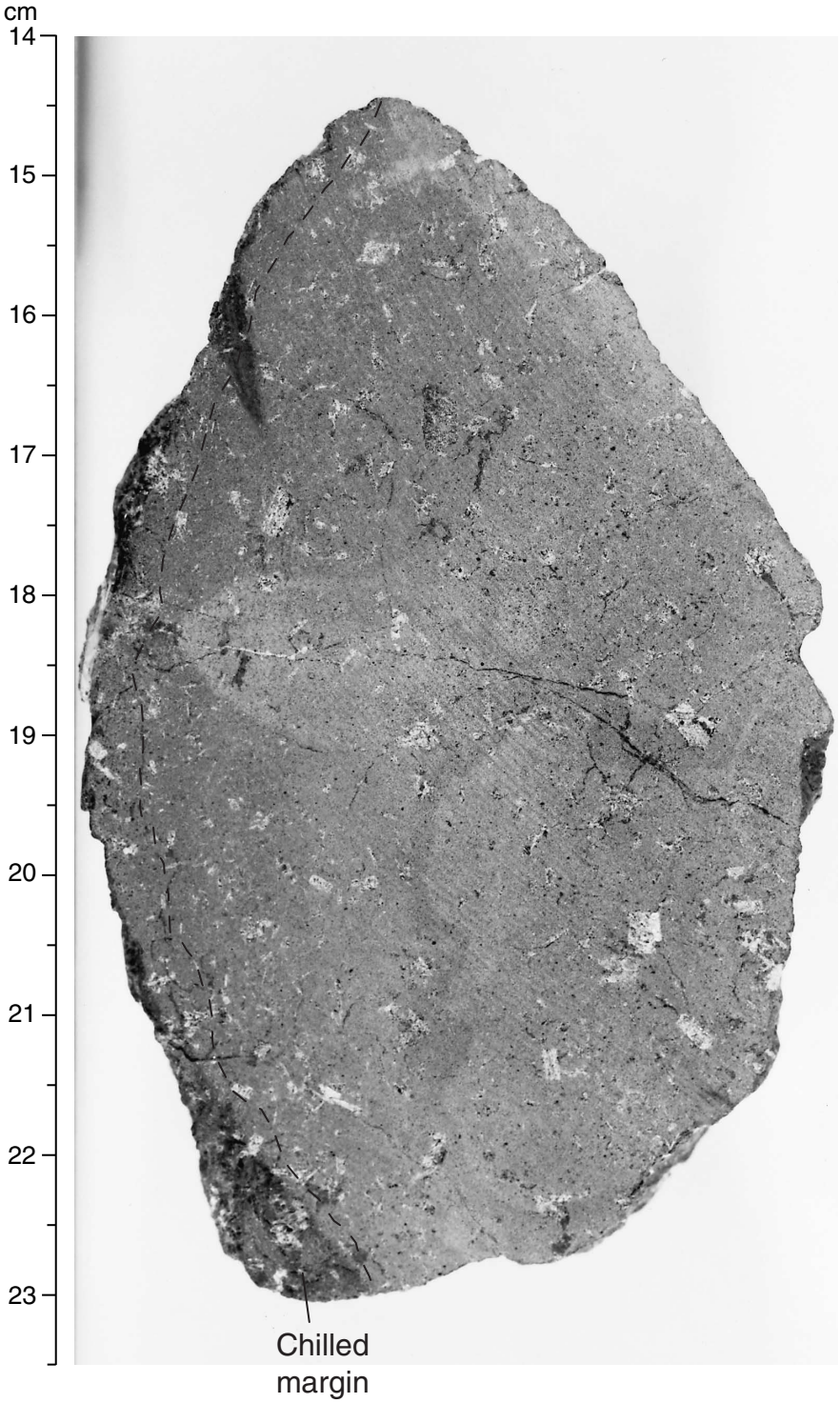

Figure F19. Photograph of outer core surface of Sample 187-1157B-3R-2, 90–93 cm, showing fragments of glass + palagonite in clay sediment.

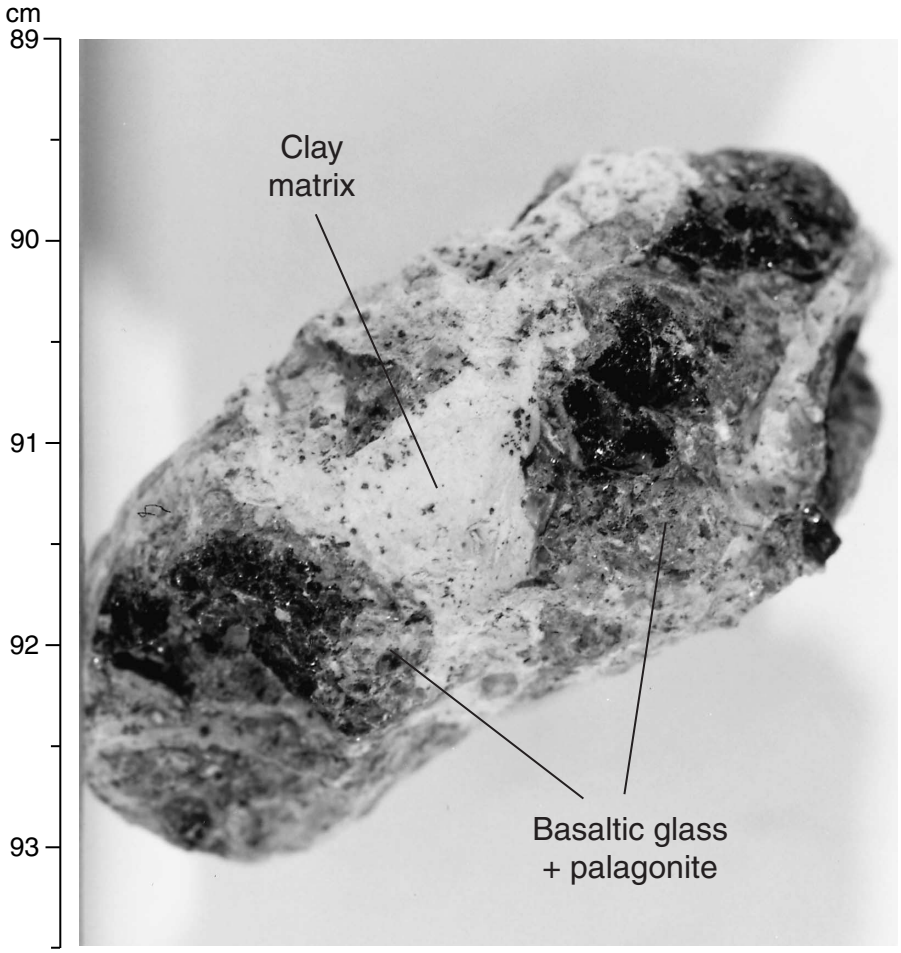

Figure F20. Photograph of interval 187-1157B-3R-2, 109–124 cm, showing an accumulation of micritic calcite sediment attached to a basalt piece that is continuous with a micritic calcite vein network running the length of the piece.

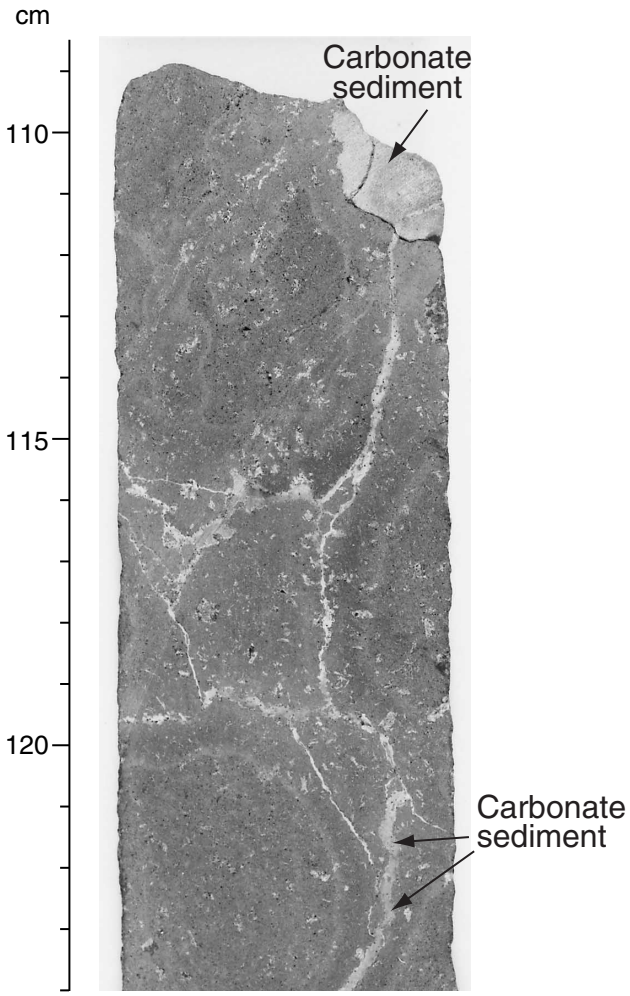

Figure F21. Photomicrograph in plane-polarized light of Sample 187-1157B-3R-1, 137–140 cm (see **"Site 1157 Thin Sections,"** p. 27), showing lithic fragments in a micritic calcite vein, including a partially disaggregated fragment of basalt probably from the wall rock (upper left) and a pseudomorph of skeletal olivine consisting of pale brown clay (lower right).

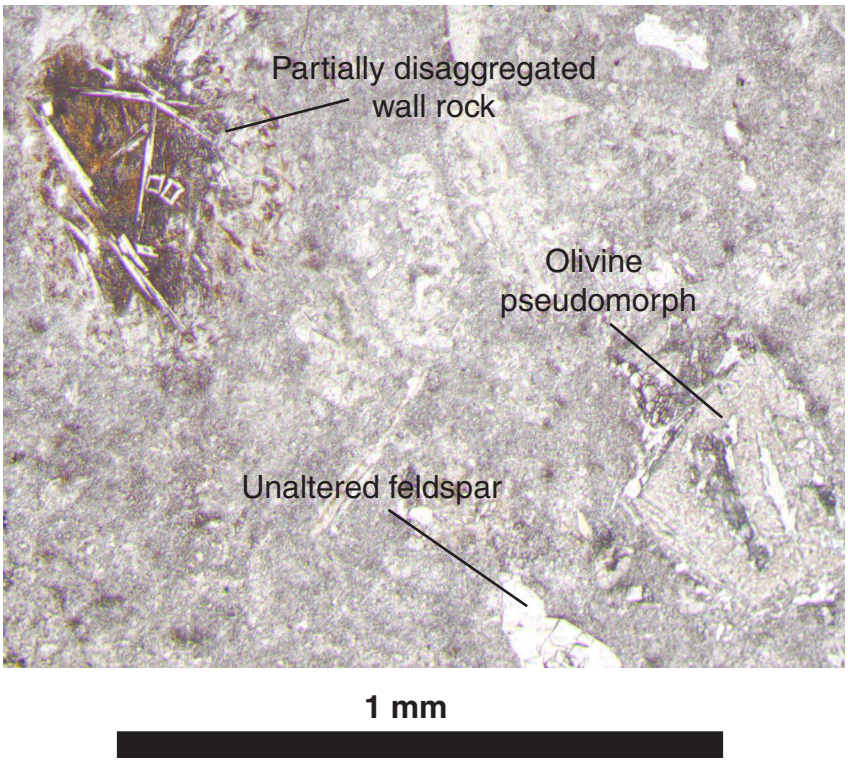

Figure F22. Photomicrograph in plane-polarized light of Sample 187-1157B-5R-1, 54–57 cm (see "Site 1157 Thin Sections," p. 28), showing a micritic calcite vein crosscutting clay-rich material adjacent to the basalt wall rock. Identifiable lithic clasts include altered and unaltered plagioclase. Note the thin sparry calcite vein that bifurcates, passing between the upper boundary of the micritic vein and the clay on one side and crosscutting the clay/basalt contact on the other. Note also the truncated plagioclase (Plag.) phenocryst (lower right). (The white space between the basalt and the micrite vein [lower right] is due to parting during preparation of the thin section and is not a calcite vein.)

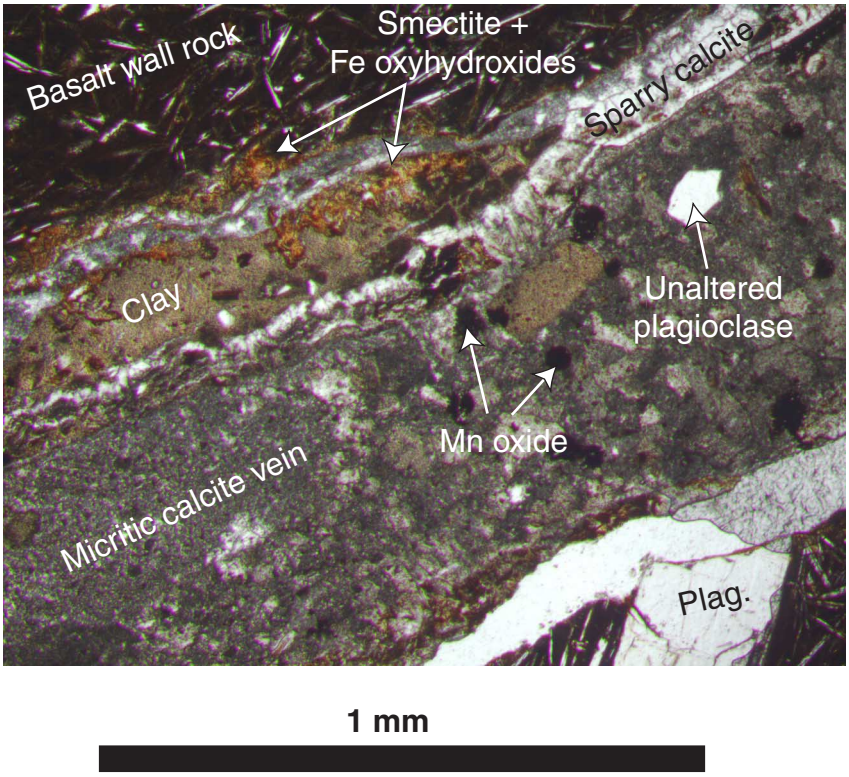

Figure F23. Photomicrograph, with crossed polars, of Sample 187-1157B-3R-1, 97–101 cm (see **"Site 1157 Thin Sections,"** p. 26), showing the boundary of a micritic vein (left) that is partially recrystallized to very finely crystalline sparry calcite (right). Note the alteration of wall-rock mineral phases to clay + fibrous amphibole and/or chlorite?. Note also the concentration of Mn-Fe oxyhydroxides + Mn oxides in the micritic part of the vein and their absence from the recrystallized calcite. (See Figure **F27,** p. 40, for another view of this section.)

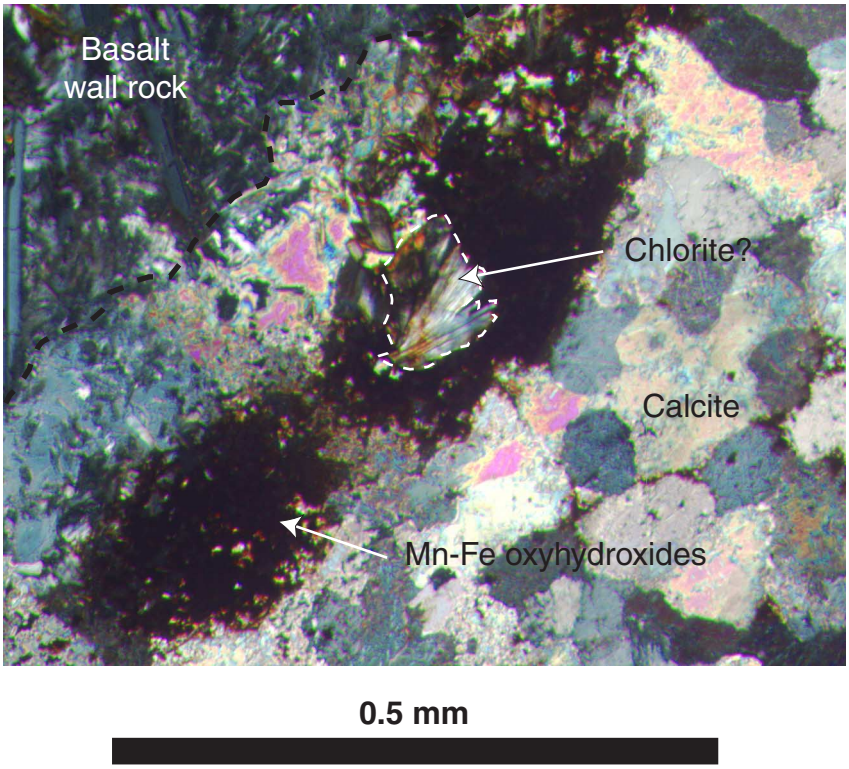

Figure F24. Photomicrograph in plane-polarized light of Sample 187-1157B-3R-1, 97–101 cm (see "Site 1157 Thin Sections," p. 26), showing a remnant of micritic calcite within a partially recrystallized, very finely crystalline sparry calcite. Note the elongation of the micritic patch parallel to the vein wall.

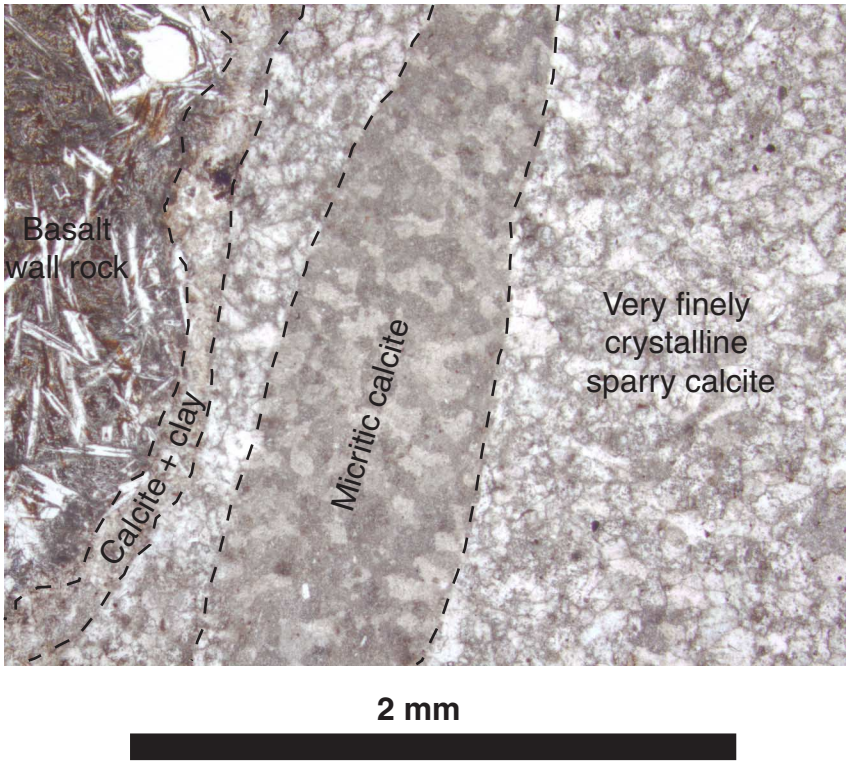

Figure F25. Photomicrograph in plane-polarized light of Sample 187-1157A-2R-1, 30–33 cm (see "Site 1157 Thin Sections," p. 20), showing a partially altered basalt glass shard in calcareous sediment. The gray patches in fresh glass are defects in the slide. Note the abundance and variety of lithic clasts.

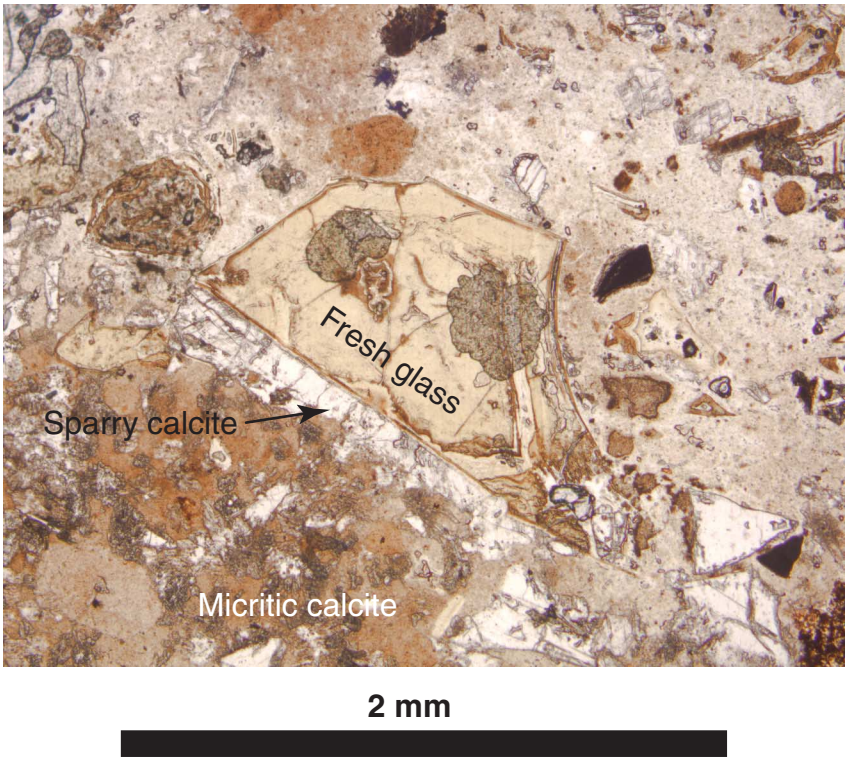

Figure F26. Photograph of interval 187-1157B-3R-1, 137–147 cm, showing calcite veins dissecting basalt. The veins are surrounded by symmetric alteration halos in which groundmass is mostly replaced by smectite, and Fe oxyhydroxide and olivine phenocrysts are iddingsitized. Note the irregular vein/wall-rock boundary. Spotty Mn oxide is common within the calcite veins.

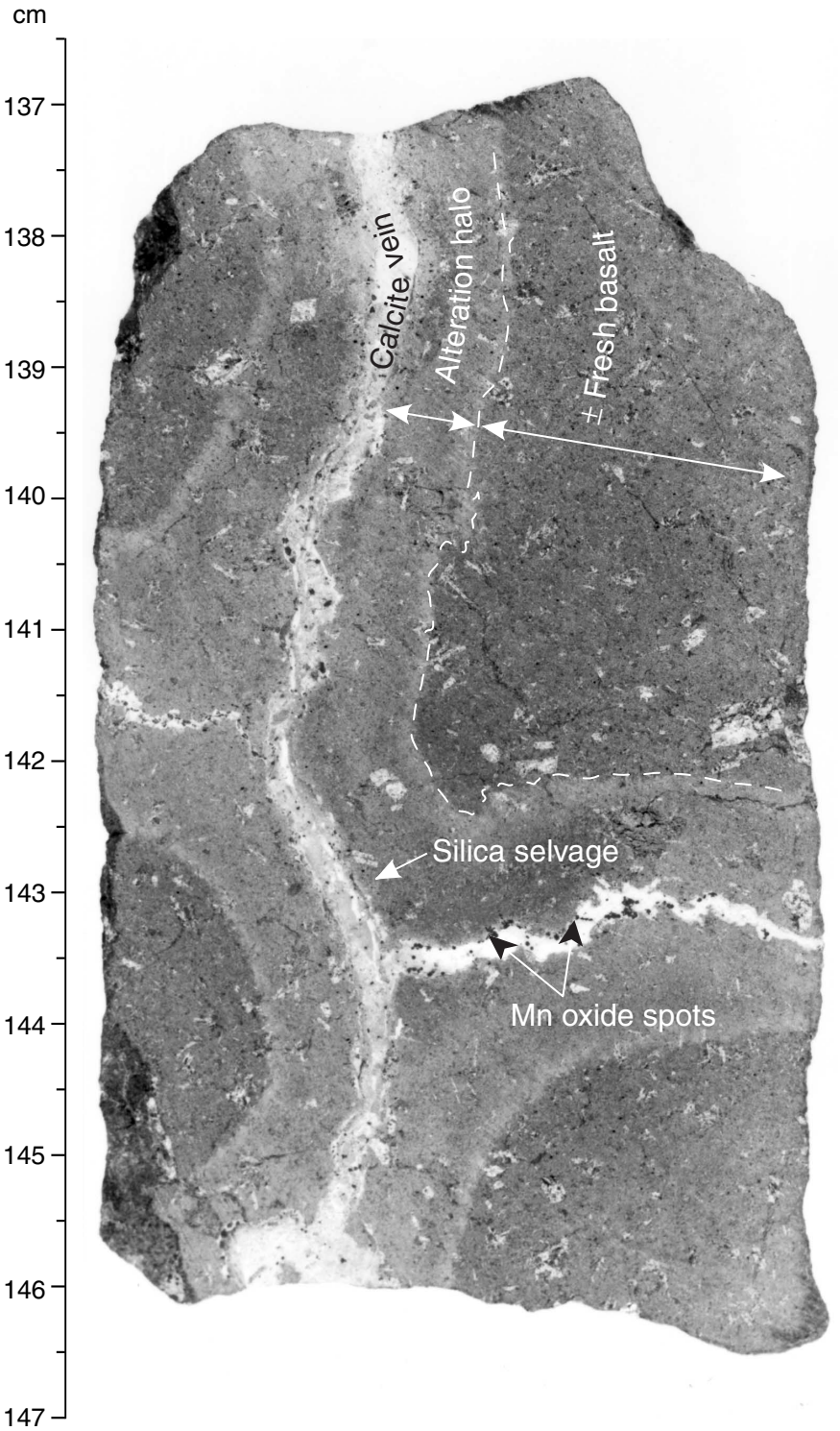

Figure F27. Photomicrograph, with crossed polars, of Sample 187-1157B-3R-1, 97–101 cm (see **"Site 1157 Thin Sections,"** p. 26), showing the boundary of a micritic vein (left) partially recrystallized to very finely crystalline sparry calcite (right). Note that Mn oxide is abundant in the micrite but absent from the recrystallized calcite. (Figure **F23,** p. 36, shows this sample with crossed polars.)

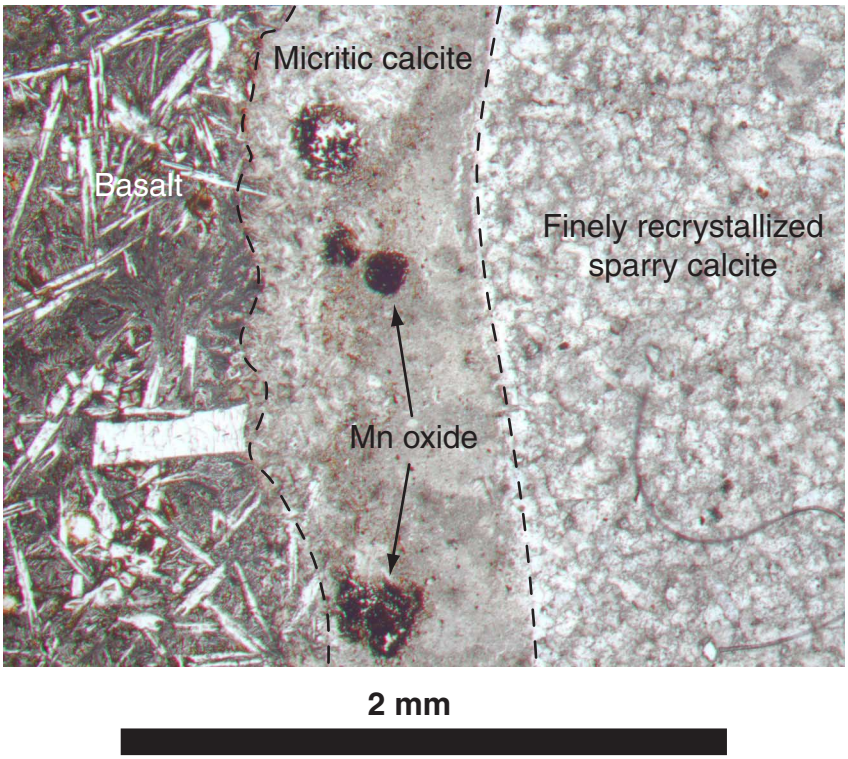

Figure F28. Photomicrograph, with crossed polars, of Sample 187-1157B-3R-1, 137–140 cm (see "Site 1157 Thin Sections," p. 27), showing a highly altered basalt clast within a micritic calcite vein. The clast probably originated from the wall rock.

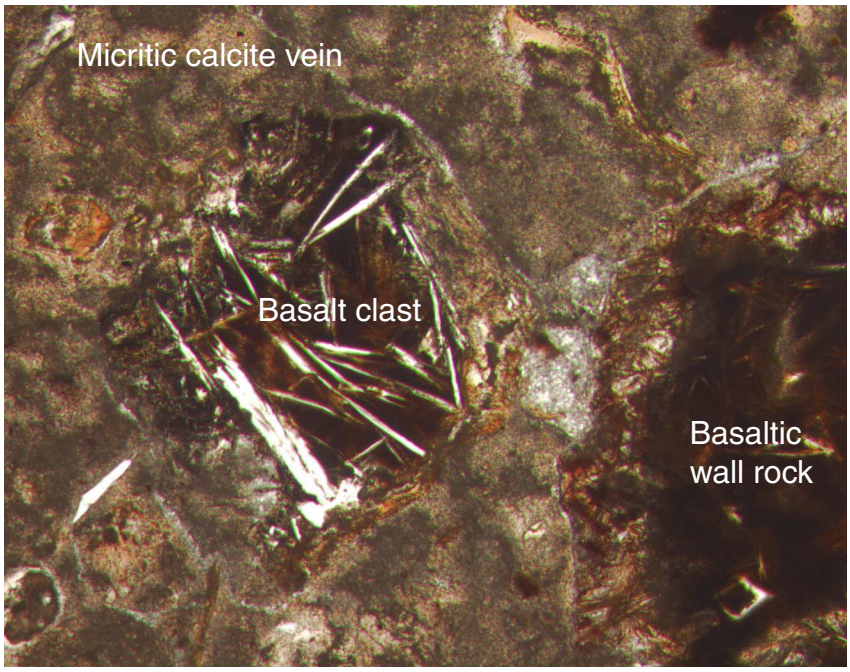

Figure F29. Photomicrograph, with crossed polars, of Sample 187-1157B-5R-1, 54–57 cm (see **"Site 1157 Thin Sections,"** p. 28), showing a basalt fragment incorporated into a calcite vein by vein propagation into the wall rock.

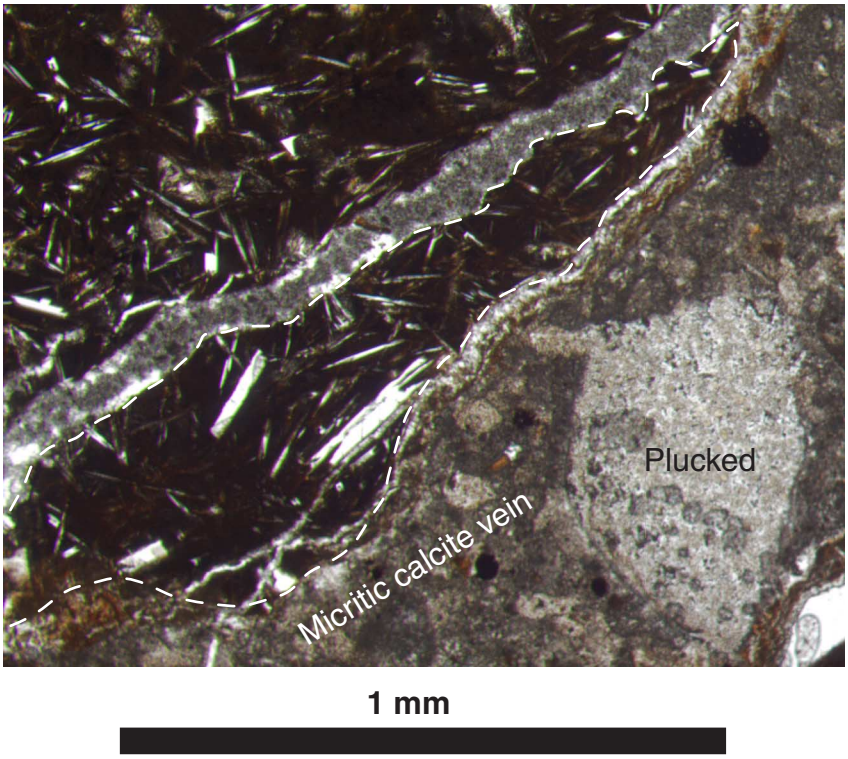

Figure F30. Photomicrograph of Sample 187-1157B-3R-1, 97–101 cm (see "Site 1157 Thin Sections," p. 26), showing an irregular sparry calcite vein boundary. Note the calcite replacement of basalt groundmass.

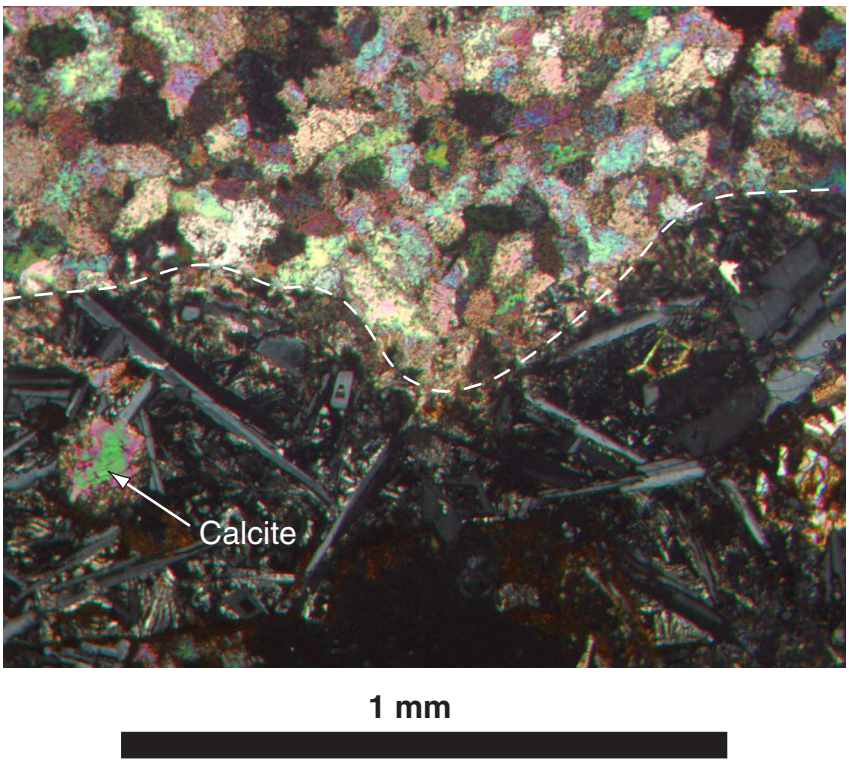

Figure F31. Photomicrograph, with crossed polars, of Sample 187-1157B-3R-1, 137–140 cm (see "Site 1157 Thin Sections," p. 27), showing a palagonite fragment (P) within a micritic calcite vein, indicating material transport into the interior of the pillow.

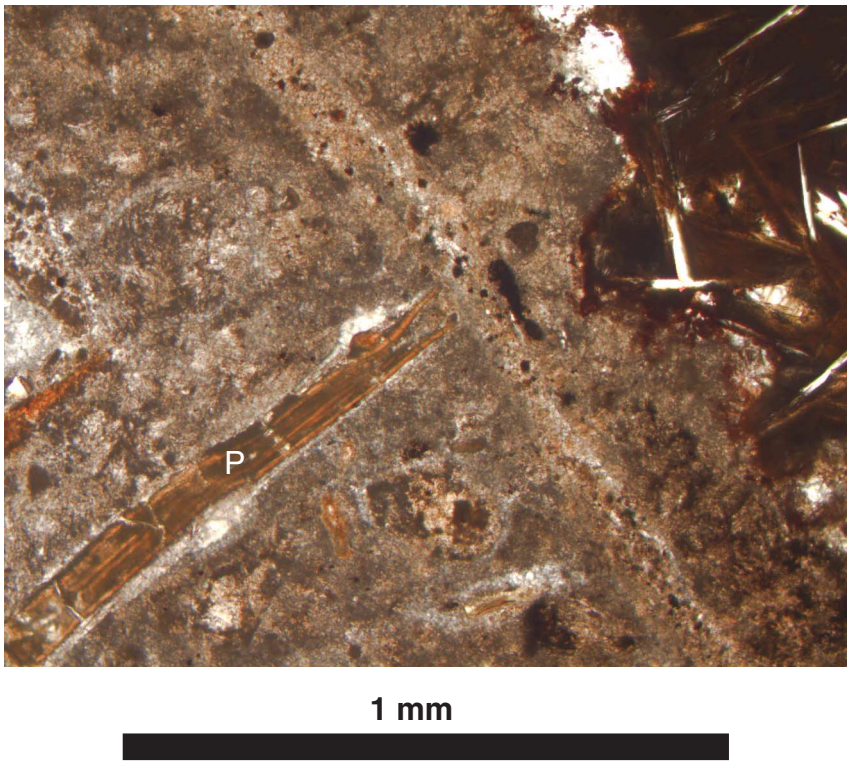

Figure F32. Photomicrograph in plane-polarized light of Sample 187-1157B-3R-1, 137–140 cm (see "Site 1157 Thin Sections," p. 27), showing a fresh plagioclase grain within a micritic calcite vein.

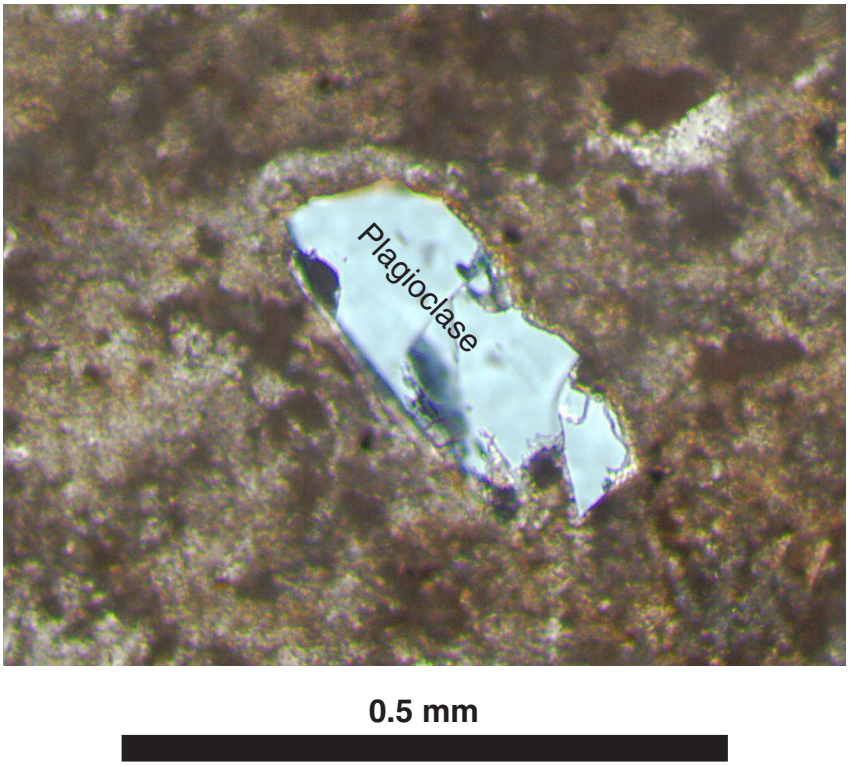

Figure F33. Photomicrograph of Sample 187-1157B-8R-2, 55–59 cm (see "Site 1157 Thin Sections," p. 30), showing calcite replacing an olivine phenocryst. Ol. = olivine.

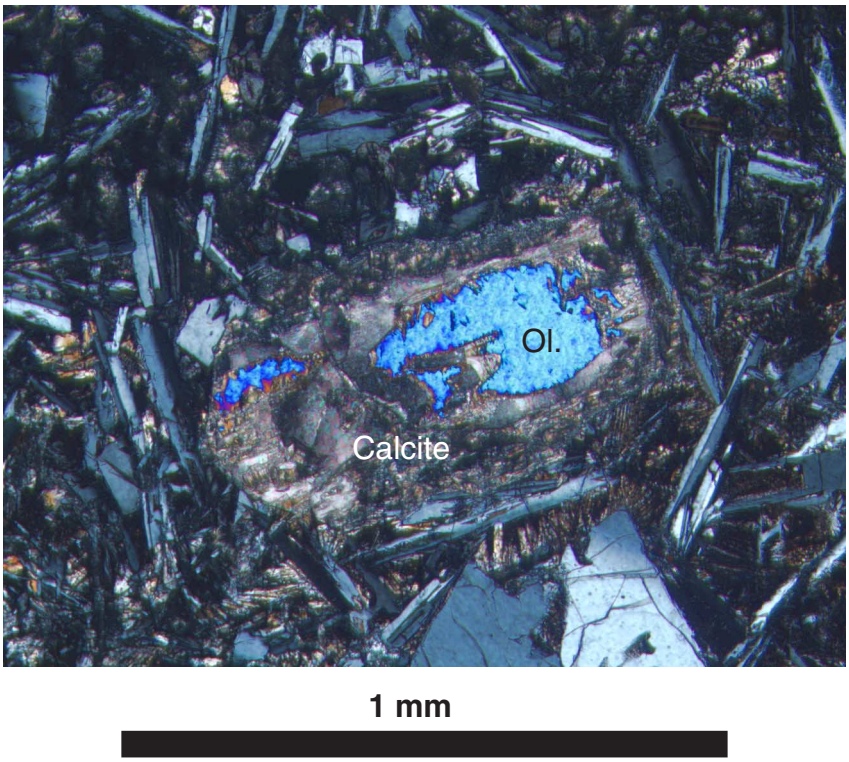

Figure F34. A plot of fracture + vein density (*N*/m = number per meter of core) calculated for each section from Site 1157. The horizontal thick line and associated number represent the average for each hole.

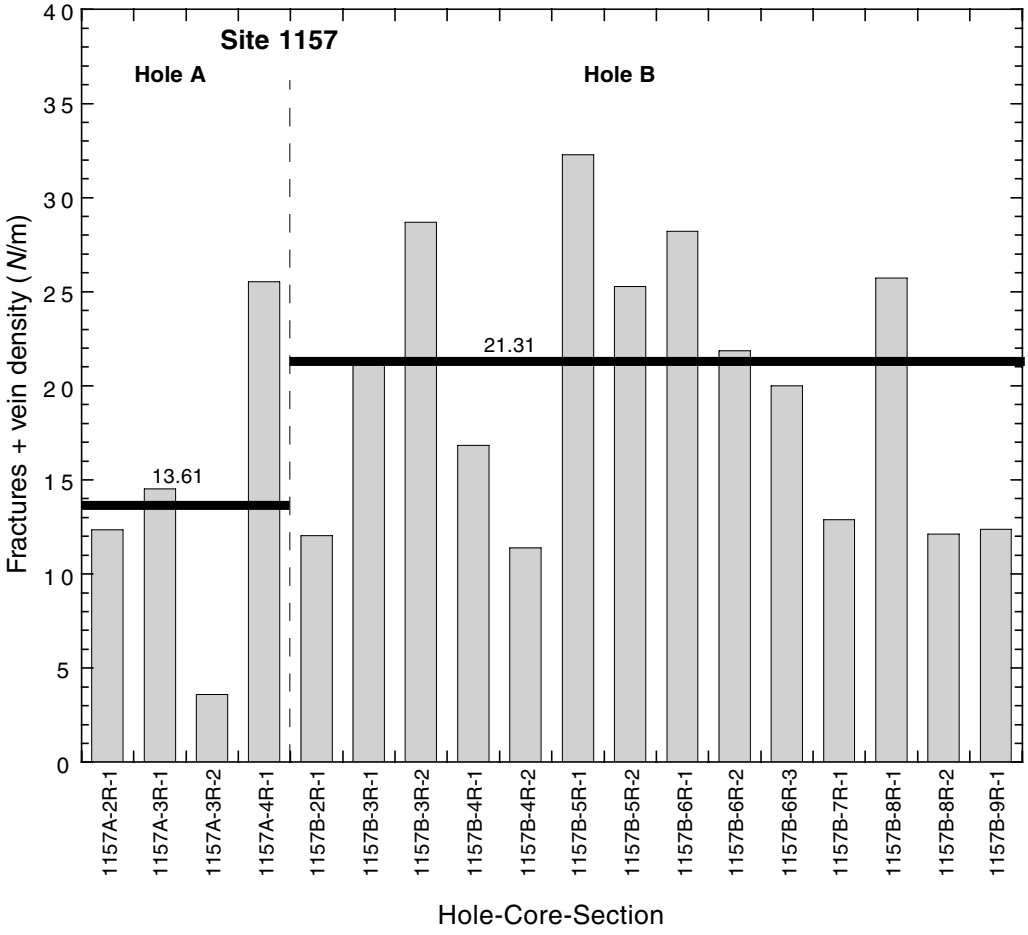

Figure F35. Track chart of the *JOIDES Resolution* single-channel seismic survey line S6. Crosses = 50-shot intervals. Holes 1157A and 1157B (solid circles) are ~2 km east of the prospectus site AAD–28a.

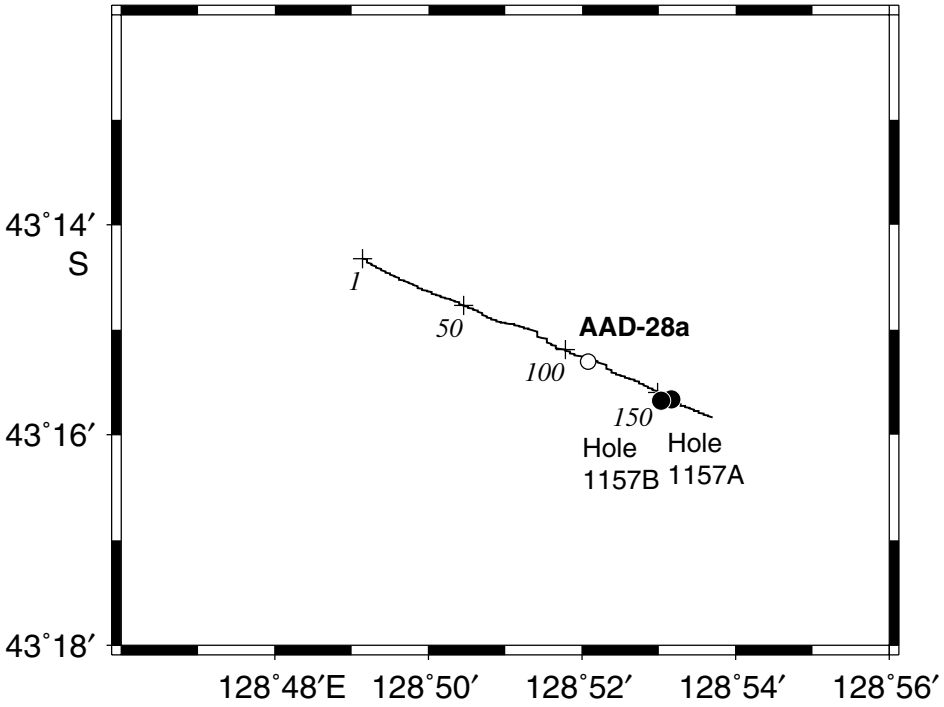

Figure F36. Single-channel seismic profile of line S6 from shotpoints 1 to 170. The large arrow marks the position of Site 1157 near shotpoint 157. Prospectus site AAD-28a is near shotpoint 115.

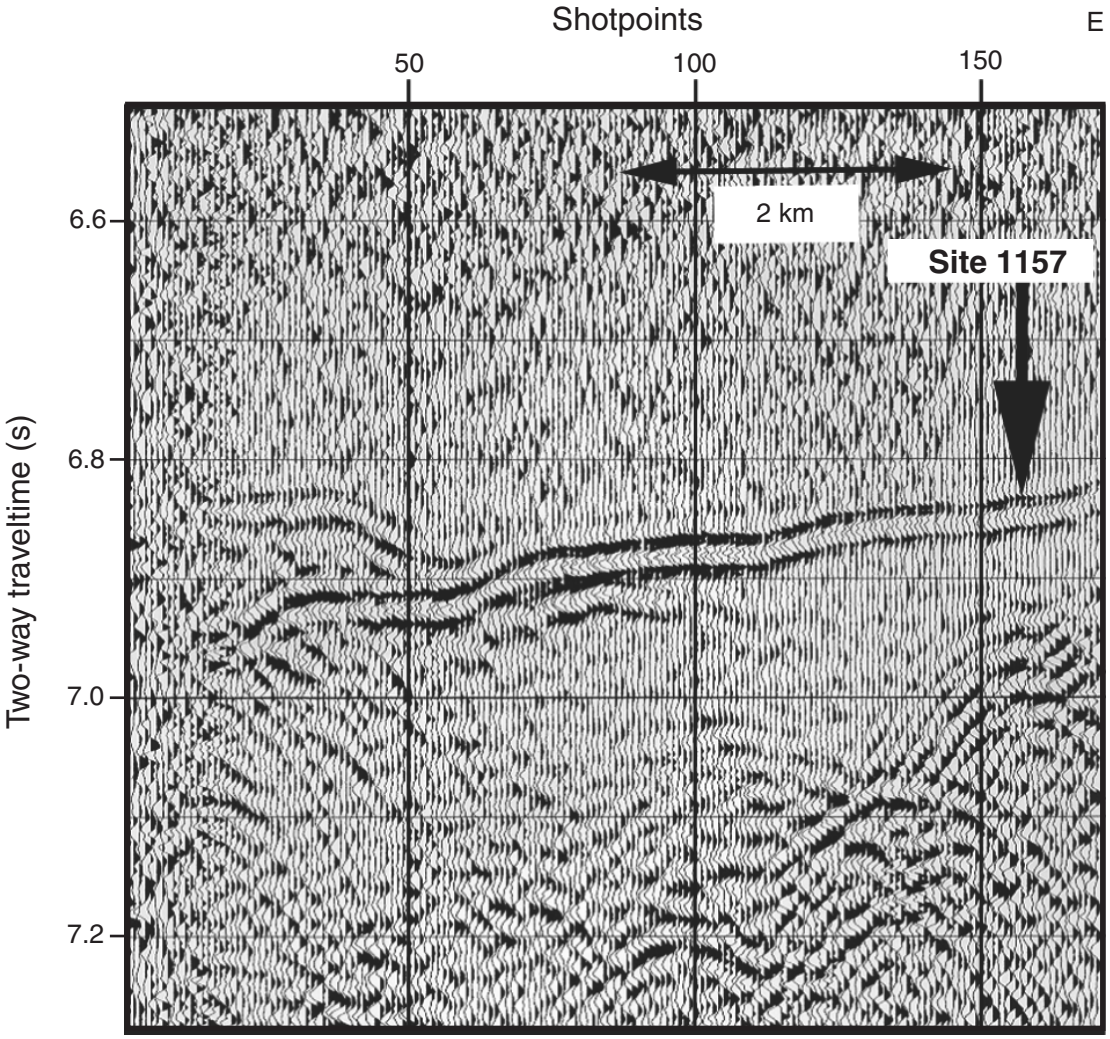

Figure F37. A schematic illustration of color variation in Core 187-1157A-1W. The locations of changes from siliceous to calcareous sediments are noted. CC = core catcher.

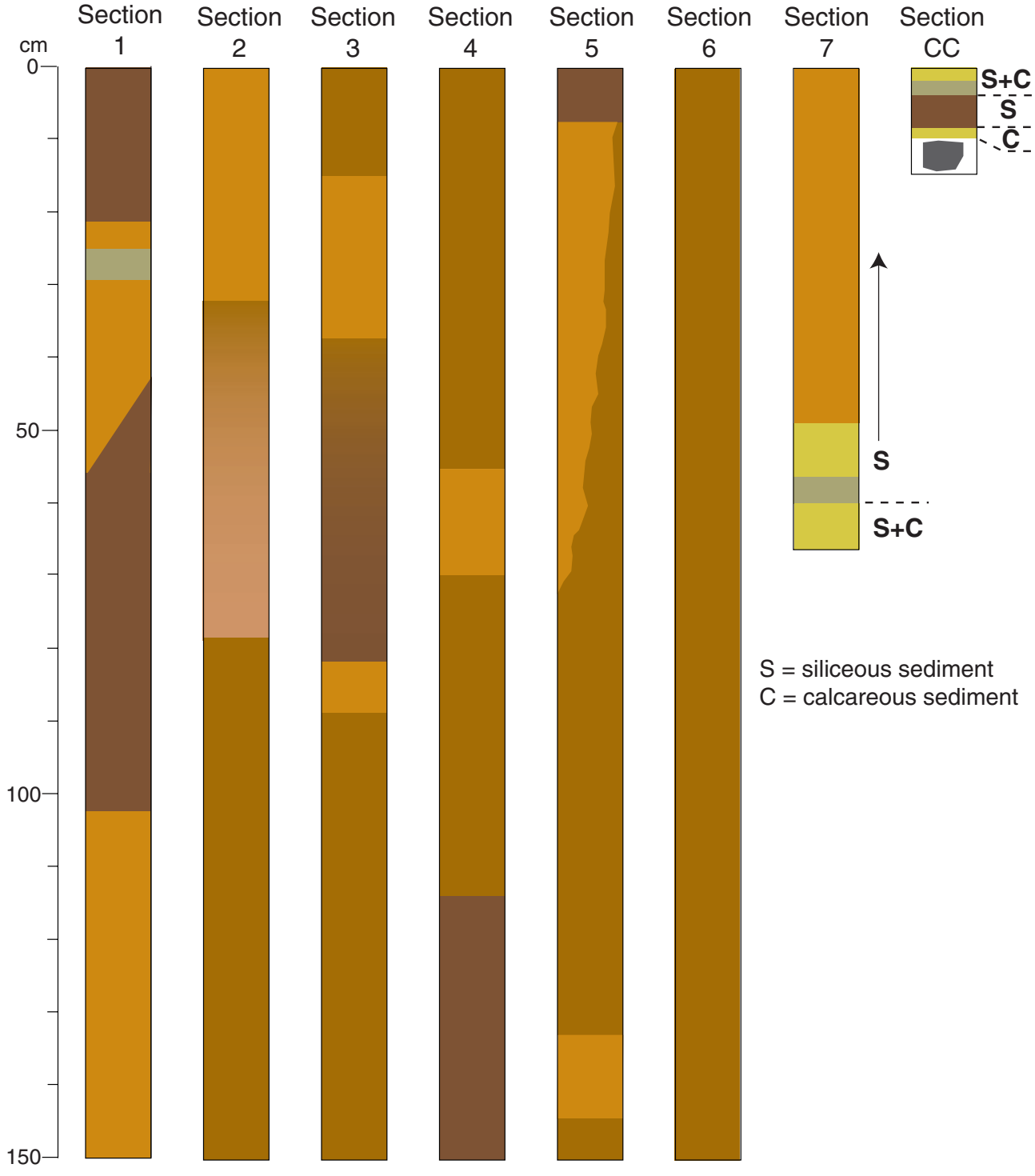

Figure F38. Major element compositions vs. MgO for Holes 1157A and 1157B basalts compared with 0- to 7-Ma Southeast Indian Ridge glasses from Zone A. Only the average X-ray fluorescence or ICP-AES analyses reported in Table T3, p. 56, are plotted.

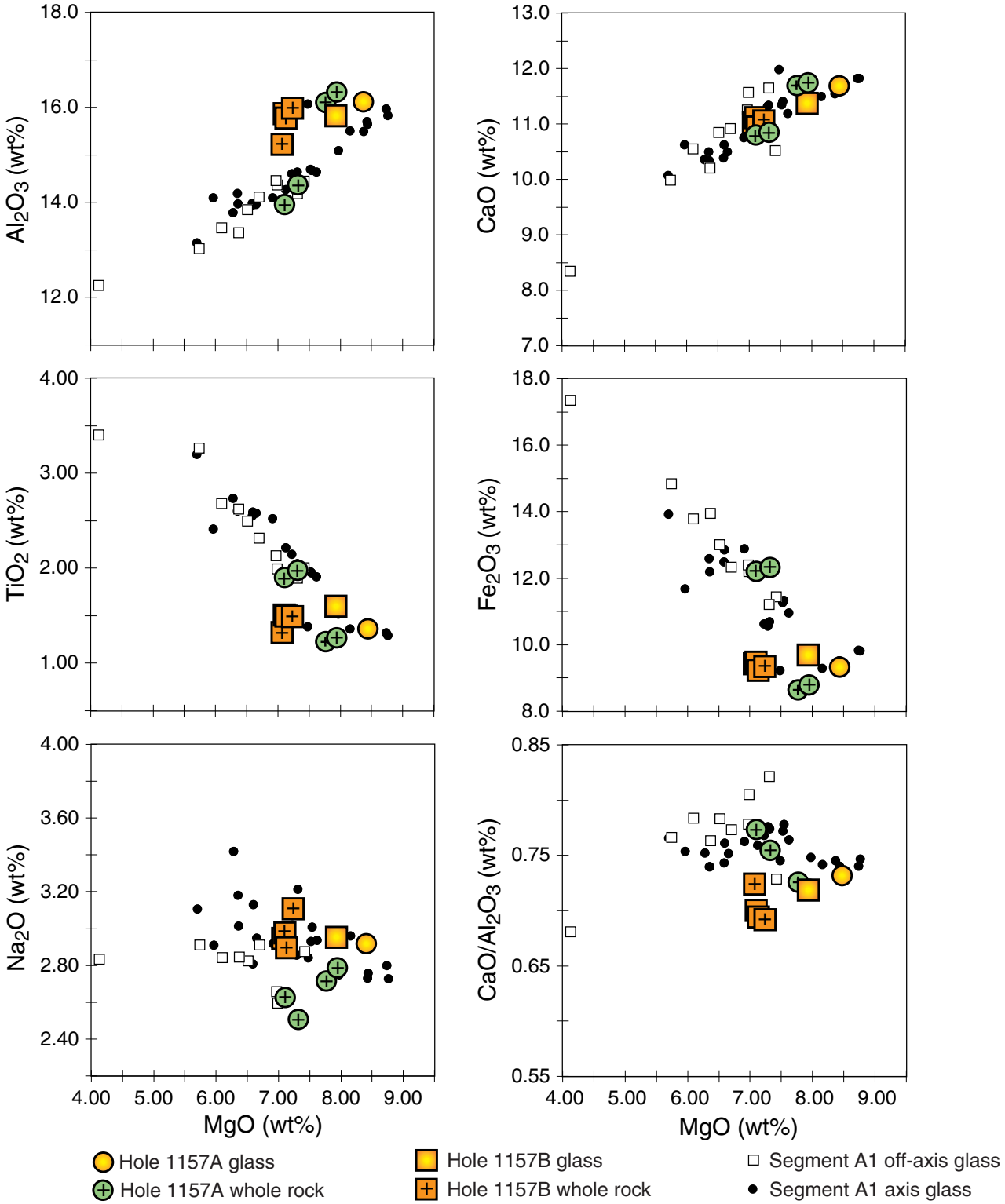

Figure F39. Trace element compositions vs. MgO for Holes 1157A and 1157B basalts compared with 0- to 7-Ma Southeast Indian Ridge glasses from Zone A. Only the average X-ray fluorescence or ICP-AES analyses reported in Table T3, p. 56, are plotted.

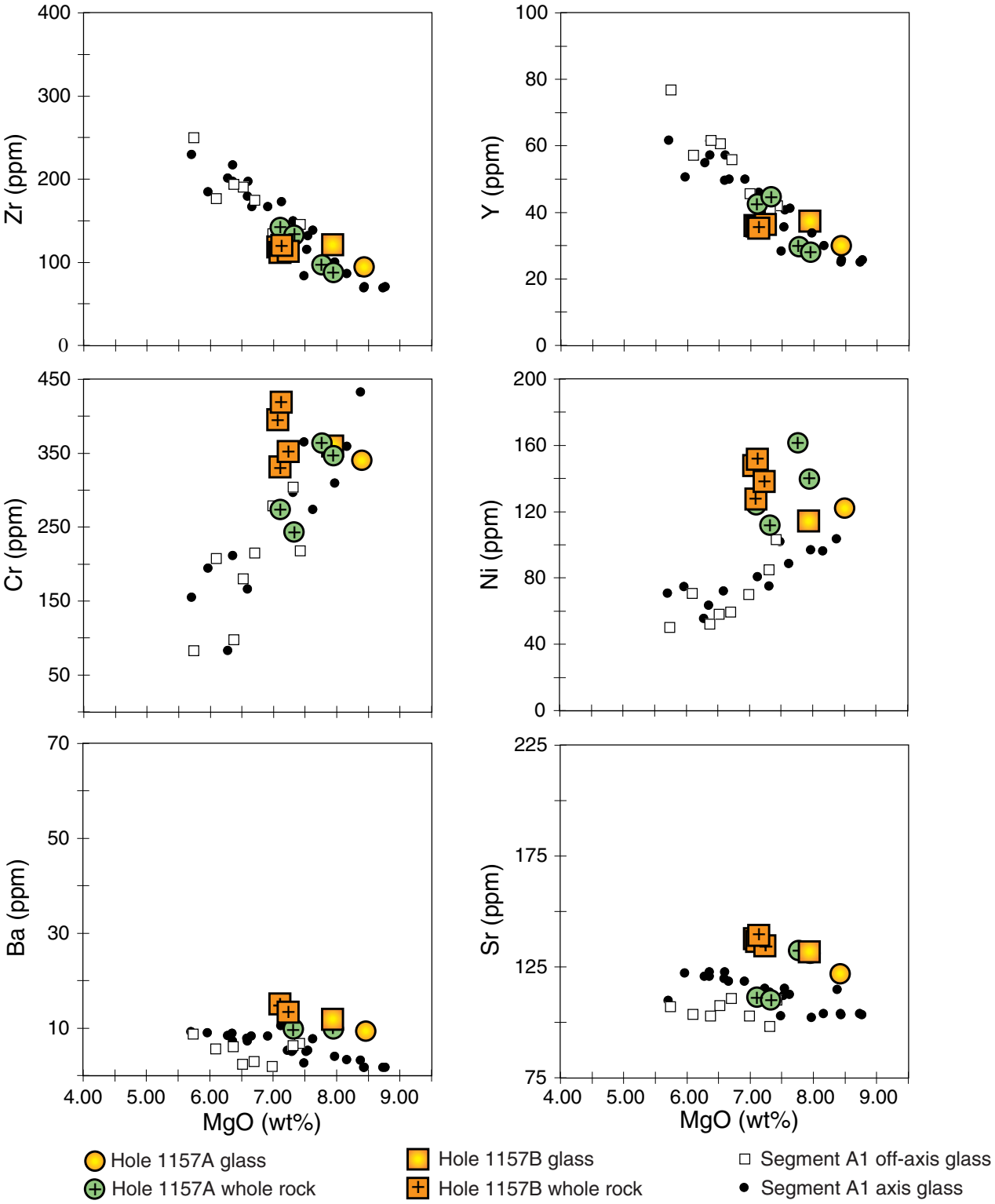

Figure F40. A. Variations of Zr/Ba vs. Ba for Hole 1157A and Hole 1157B basaltic glass and whole-rock samples compared with Indian- and Pacific-type mid-ocean-ridge basalt (MORB) fields defined by 0- to 7-Ma Southeast Indian Ridge (SEIR) lavas dredged between 123°E and 133°E. TP = Transitional Pacific; PRT = propagating rift tip lavas. **B.** Variations of Na_2O/TiO_2 vs. MgO for Hole 1157A and Hole 1157B basaltic glass and whole-rock samples compared with Indian- and Pacific-type MORB fields defined by zero-age SEIR lavas dredged between 123°E and 133°E. Dashed line separates Indian- and Pacific-type zero-age SEIR basalt glass.

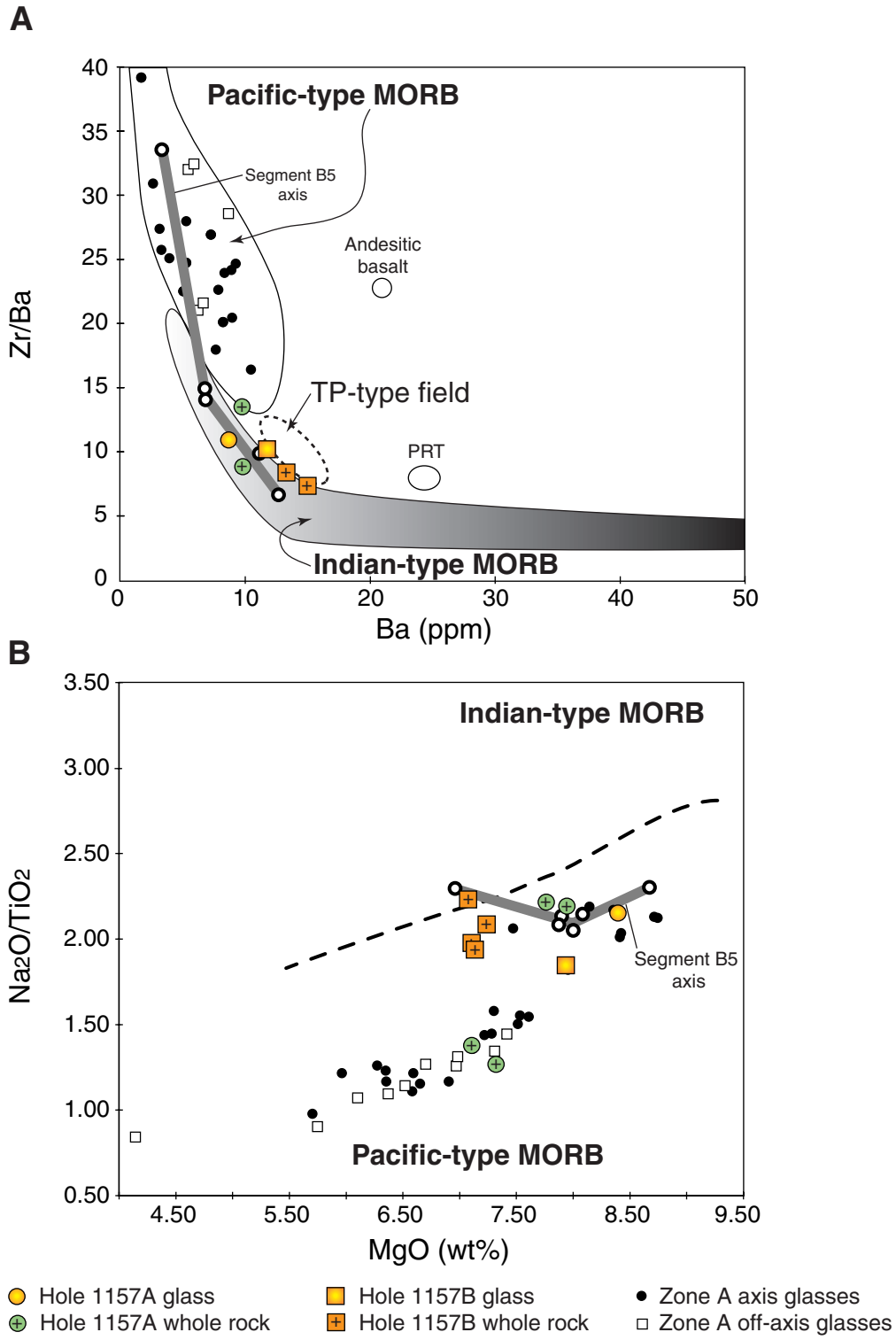

Table T1. Coring summary, Site 1157.

Hole 1157A
Latitude: 43°15.6639′S
Longitude: 128°53.1660′E
Time on hole: 1415 hr, 12 Dec 99–1300 hr, 13 Dec 99 (22.75 hr)
Time on site: 1415 hr, 12 Dec 99–1100 hr, 15 Dec 99 (68.75 hr)
Seafloor (drill-pipe measurement from rig floor, mbrf): 5080.4
Distance between rig floor and sea level (m): 11.1
Water depth (drill-pipe measurement from sea level, m): 5069.3
Total depth (from rig floor, mbrf): 5296.8
Total penetration (mbsf): 216.4
Total length of cored section (m): 16.4
Total length of drilled intervals (m): 200.0
Total core recovered (m): 2.92
Core recovery (%): 17.8
Total number of cores: 3
Total number of drilled cores: 1

Hole 1157B
Latitude: 43°15.6758′S
Longitude: 128°53.0295′E
Time on hole: 1300 hr, 13 Dec 99–1100 hr, 15 Dec 99 (46.0 hr)
Seafloor (drill-pipe measurement from rig floor, mbrf): 5069.3
Distance between rig floor and sea level (m): 11.1
Water depth (drill-pipe measurement from sea level, m): 5058.2
Total depth (from rig floor, mbrf): 5251.4
Total penetration (mbsf): 171.0
Total length of cored section (m): 40.4
Total length of drilled intervals (m): 130.6
Total core recovered (m): 11.7
Core recovery (%): 29.0
Total number of cores: 8
Total number of drilled cores: 1

Core	Date (Dec 1999)	Ship local time	Depth (mbsf) Top	Depth (mbsf) Bottom	Length (m) Cored	Length (m) Recovered	Recovery (%)	Comment
187-1157A-								
1W	13	0430	0.0	200.0	200.0	9.82	N/A	
2R	13	0710	200.0	206.0	6.0	0.77	12.8	Whirl-Pak
3R	13	1005	206.0	215.4	9.4	1.63	17.3	
4R	13	1155	215.4	216.4	1.0	0.52	52.0	
				Cored:	16.4	2.92	17.8	
				Drilled:	200.0			
				Total:	216.4			
187-1157B-								
1W	13	1820	0.0	130.6	130.6	0.00	N/A	
2R	13	2335	130.6	138.5	7.9	1.12	14.2	Whirl-Pak
3R	14	0230	138.5	143.0	4.5	2.21	49.1	
4R	14	0535	143.0	147.8	4.8	1.80	37.5	
5R	14	0810	147.8	152.2	4.4	1.77	40.2	
6R	14	1115	152.2	157.2	5.0	2.41	48.2	
7R	14	1545	157.2	161.4	4.2	0.38	9.0	
8R	14	2040	161.4	166.4	5.0	1.60	32.0	
9R	15	0145	166.4	171.0	4.6	0.41	8.9	Whirl-Pak
				Cored:	40.4	11.70	29.0	
				Drilled:	130.6			
				Total:	171.0			

Notes: N/A = not applicable. This table is also available in ASCII format.

Table T2. Rock samples incubated for enrichment cultures and prepared for DNA analysis and electron microscope studies and microspheres evaluated for contamination studies.

Core	Depth (mbsf)	Sample type	Enrichment cultures				DNA analysis		SEM/TEM samples	Microspheres†	
			Anaerobic	Aerobic	Microcosm*	High pressure	Wash	Fixed	Air dried	Exterior	Interior
187-1157A-											
2R	200.0-206.0									Yes	Yes
3R	206.0-215.4	Breccia	9	3	1 Mn	X	X	X	X		
187-1157B-											
2R	130.6-138.5	Fine-grained basalt	8	3	1 Fe/S	X	X	X	X	Yes	Yes
4R	143.0-147.8	Chilled margin	8	3	1 Fe/S		X	X	X		
8R	161.4-166.4	Chilled margin	9	3		X	X	X	X	Yes	Yes

Notes: * = microcosm for iron and sulfur (Fe/S) or manganese (Mn) redox cycles; SEM = scanning electron microscope; TEM = transmission electron microscopy; † = contamination test; X = samples prepared on board. This table is also available in **ASCII** format.

Table T3. Glass and whole-rock major and trace element compositions of basalts, Site 1157.

	Hole 1157A												Hole 1157B									
Core, section:	1W-CC	1W-CC	1W-CC	1W-CC	2R-1	2R-1	2R-1	2R-1	3R-2	3R-2	3R-2	3R-2	3R-1	3R-1	3R-1	3R-1	4R-1	4R-1	6R-1	6R-1	6R-1	6R-1
Interval (cm):	13-17	13-17	13-17	13-17	86-90	86-90	86-90	86-90	19-22	19-22	19-22	19-22	62-67	62-67	62-67	62-67	136-138	136-138	43-47	43-47	43-47	43-47
Depth (mbsf):	9.78	9.78	9.78	9.78	200.86	200.86	200.86	200.86	207.69	207.69	207.69	207.69	139.12	139.12	139.12	139.12	144.36	144.36	152.63	152.63	152.63	152.63
Piece:	1	1	1	1	16	16	16	16	3B	3B	3B	3B	9	9	9	9	17	17	7	7	7	7
Analysis:	ICP	ICP	ICP	ICP	XRF	XRF	ICP	ICP	XRF	XRF	ICP	ICP	XRF	XRF	ICP	ICP	ICP	ICP	XRF	XRF	ICP	ICP
Rock type:	Glass	Glass	Glass	Glass	Aphyric basalt				Sparsely to moderately plagioclase-olivine phyric basalt				Moderately plagioclase-olivine phyric basalt				Glass	Glass	Moderately plagioclase-olivine phyric basalt			
Major element (wt%)																						
SiO_2	52.60	51.54	51.35	52.03	48.13	47.84	48.40	51.05	48.71	48.34	49.56	50.47	48.94	48.23	49.87	50.53	52.31	52.14	49.17	49.30	50.54	50.45
TiO_2	1.47	1.37	1.40	1.43	1.87	1.94	1.92	2.03	1.24	1.21	1.25	1.29	1.28	1.36	1.50	1.51	1.58	1.62	1.47	1.52	1.51	1.46
Al_2O_3	16.20	15.72	15.98	16.22	13.98	13.94	14.22	14.53	16.13	16.09	16.05	16.60	15.28	15.16	15.81	15.92	15.69	15.94	15.76	15.79	15.99	15.97
Fe_2O_3	9.87	9.45	9.10	9.35	12.21	12.20	12.07	12.59	8.62	8.66	8.70	8.88	9.43	9.40	9.45	9.47	9.59	9.77	9.21	9.24	9.35	9.34
MnO	0.16	0.15	0.16	0.16	0.17	0.18	0.18	0.20	0.13	0.13	0.14	0.15	0.11	0.12	0.15	0.15	0.16	0.16	0.14	0.15	0.16	0.15
MgO	8.92	8.31	8.24	8.47	7.13	7.08	7.19	7.45	7.77	7.76	7.86	8.03	7.12	7.03	7.13	7.09	7.96	7.92	7.13	7.14	7.34	7.14
CaO	12.08	11.64	11.37	11.70	10.84	10.76	10.84	10.87	11.72	11.67	11.68	11.81	11.09	10.94	11.08	11.13	11.36	11.37	10.96	10.93	11.13	10.96
Na_2O	2.98	2.82	2.95	3.05	2.70	2.55	2.71	2.30	2.67	2.76	2.85	2.73	2.98	2.91	3.14	2.81	2.92	2.98	2.95	2.84	3.13	3.08
K_2O	0.13	0.11	0.13	0.13	0.26	0.26	0.26	0.22	0.24	0.24	0.25	0.23	0.20	0.21	0.24	0.23	0.10	0.10	0.24	0.25	0.25	0.25
P_2O_5	0.17	0.15	0.14	0.16	0.19	0.19	0.23	0.16	0.13	0.13	0.15	0.13	0.15	0.15	0.18	0.15	0.18	0.17	0.15	0.15	0.17	0.16
LOI					0.65	0.65			0.95	0.95			0.87	0.87					0.77	0.77		
CO_2																						
H_2O																						
Total:	104.59	101.26	100.82	102.70	98.13	97.59	98.03	101.40	98.31	97.94	98.49	100.32	97.45	96.38	98.54	99.01	101.83	102.18	97.95	98.08	99.59	98.98
Trace element (ppm)																						
Nb					6				6				6						5			
Zr	105	93	112	101	142		141	125	97		89	86	118		114	108	123	119	120		115	111
Y	32	30	34	35	43		47	42	30		29	27	36		37	35	38	37	35		37	35
Sr	132	117	111	126	111		110	111	132		130	132	138		138	135	131	132	139		135	134
Rb					3				3				2						3			
Zn					101				70				80						80			
Cu					62				60				56						59			
Ni	131	122	120	120	124		119	105	162		143	136	148		133	122	113	116	151		139	137
Cr	367	311	349	362	274		253	234	364		347	346	395		340	323	362	356	418		355	348
V					337				162				249						254			
Ce					35				18				32						33			
Ba	10	8	9	10			10	10			10	10			15	15	12	12			13	13
Sc	35	32	38	35			39	43			30	36			34	38	36	37			36	36

Notes: CC = core catcher; LOI = loss on ignition. This table is also available in **ASCII** format.